Lecture Note #3 (Fall, 2022)

Experimental Probes and Techniques

1. Ultrahigh vacuum, light sources (X-ray)
2. Probe techniques
3. Electron diffraction
4. Electron spectroscopy
5. Vibrational spectroscopy

Reading: Kolasinski, ch.2

The techniques of surface science

- AES, AFM, EELS, XPS(ESCA), EXAFS, FEM, FIM, FTIR, HEIS, APXPS, HREELS, IRAS, ISS, LEED, LEIS, NEXAFS, NMR, RBS, SEM, SERS, SFG, SHG, SIMS, STM, TEM, TDS, UPS, XANES, SPS, XRD… (see Table 1.1)

- Surface properties: structure, composition, oxidation states, chemical properties, electronic properties, mechanical properties → atomic resolution, smaller energy resolution, shorter time scales, *in situ*, high pressure

- Sources: electron, atoms, ions, photons(X-ray, UV, visible, IR…)

TEM
SEM
TED
EELS
AES
LEED

XRD
XPS
UPS
EXAFS
XANES
IR

Ultrahigh vacuum (UHV)

- Ultra-high vacuum (UHV) conditions → atomically clean surfaces

the Flux, F, of molecules striking the surface of unit area at pressure P

M: average molecular weight of gases species, N_A: Avogadro's number
$m = M/N_A$, $k_B = R/N_A$

$$Z_w = P/(2\pi m k_B T)^{1/2}$$ (1.0.1) in textbook

1 • UHV (<1.33 x 10^{-7} Pa = 10^{-9} Torr) → to maintain a clean surface for ~ 1h

2 • Mean free path: distance that a particle travels on average between collisions → longer mean free path for electron in e^- spectroscopy

The mean free path is the distance that a particle travels on average between collisions. In an ideal gas with mean velocity $\bar{c}$ and collision frequency Z, its value is given by

$$\lambda = \frac{\bar{c}}{Z} = \frac{k_B T}{2^{1/2}\sigma p} \qquad (2.1.3)$$

The collision cross section of N_2 is $\sigma = 0.43\ \text{nm}^2$. Therefore, at a pressure of $p = 1$ atm = 101 325 Pa = 760 torr, the mean free path is just 70 nm; whereas at 1×10^{-10} torr = 1.3×10^{-13} atm = 1.3×10^{-8} Pa, the mean free path is over 500 km. In electron spectroscopy, an electron must transit from the sample to a detector without scattering from any background gas over a flight path on the order of 1 m. Therefore, electron spectroscopy generally must be performed at a pressure below 7×10^{-3} Pa (5×10^{-5} torr), such that $\lambda \geq 1$ m. In practise, even lower pressures are often required so that detector noise from electron multipliers is reduced to acceptable levels.

Light source

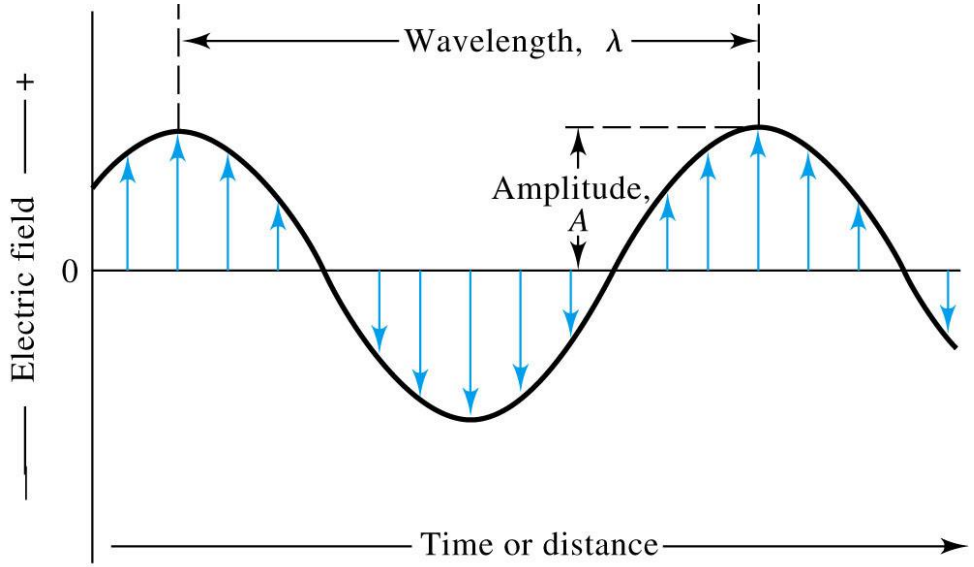

$$v_i = v\lambda_i \qquad (6\text{-}1)$$

velocity of propagation v_i
frequency v: number of oscillations per second

In a vacuum, v_i is independent of wavelength and a maximum
→ c = 2.99792 x 10^8 m/s

In a air, v_i differs only slightly from c (about 0.03% less): ~ c

$$c = v\lambda = 3.00 \times 10^8 \text{ m/s} = 3.00 \times 10^{10} \text{ cm/s} \qquad (6\text{-}2)$$

wavenumber $\bar{v}$: the reciprocal of wavelength in cm (cm^{-1})

$$E = hv = h(c/\lambda) = hc\bar{v}$$

Fundamental Constants

Constant	Symbol	Value
Speed of light	c	2.998×10^{10} cm/sec $= 2.998 \times 10^{8}$ m/sec
Planck's constant	h	6.626×10^{-27} erg · sec $= 6.626 \times 10^{-34}$ J · sec
Avogadro's number	N_A	6.022×10^{23} molecules/mole
Electron charge	e	1.602×10^{-21} coulombs $= 4.803 \times 10^{-10}$ esu
Gas constant	R	1.987 cal/deg/mole $=$ 8.315 J/deg/mole
Boltzmann's constant	k_B	1.381×10^{-16} erg/deg $= 1.381 \times 10^{-23}$ J/deg $= R/N_A$
Gravitational constant	g	9.807 m/sec^2
Permittivity of vacuum	ϵ_0	8.854×10^{-12} C^2/J/m

Energy

1 eV	1.602176×10^{-19} J
1 eV/hc	8065.5 cm^{-1}
1 meV/hc	8.0655 cm^{-1}
1 eV/particle	96.485 kJ mol^{-1}
1 kcal mol^{-1}	4.184 kJ mol^{-1}

Visible: 400~700 nm (1.8~3.1 eV)
UV: 200~400 nm (3.1~6.2 eV)
X-ray: 0.01~10 nm
(125~125,000 eV)

Energy Conversion Table[a]

	erg	joule	cal	eV	cm^{-1}
1 erg	1	10^{-7}	2.389×10^{-8}	6.242×10^{11}	5.034×10^{15}
1 joule	10^{7}	1	0.2389	6.242×10^{18}	5.034×10^{22}
1 cal	4.184×10^{7}	4.184	1	2.612×10^{19}	2.106×10^{23}
1 eV	1.602×10^{-12}	1.602×10^{-19}	3.829×10^{-20}	1	8066.0
1 cm^{-1}	1.986×10^{-16}	1.986×10^{-23}	4.747×10^{-24}	1.240×10^{-4}	1

[a] For example, 1 erg $= 2.389 \times 10^{-8}$ cal.

TABLE 6-1 Common Spectroscopic Methods Based on Electromagnetic Radiation

Type of Spectroscopy	Usual Wavelength Range*	Usual Wavenumber Range, cm^{-1}	Type of Quantum Transition
Gamma-ray emission	0.005–1.4 Å	—	Nuclear
X-ray absorption, emission, fluorescence, and diffraction	0.1–100 Å	—	Inner electron
Vacuum ultraviolet absorption	10–180 nm	1×10^6 to 5×10^4	Bonding electrons
Ultraviolet-visible absorption, emission, and fluorescence	180–780 nm	5×10^4 to 1.3×10^4	Bonding electrons
Infrared absorption and Raman scattering	0.78–300 μm	1.3×10^4 to 3.3×10^1	Rotation/vibration of molecules
Microwave absorption	0.75–375 mm	13–0.03	Rotation of molecules
Electron spin resonance	3 cm	0.33	Spin of electrons in a magnetic field
Nuclear magnetic resonance	0.6–10 m	1.7×10^{-2} to 1×10^3	Spin of nuclei in a magnetic field

Skoog, Holler, Crouch, *Principles of Instrumental Analysis* (Thomson)

X-ray

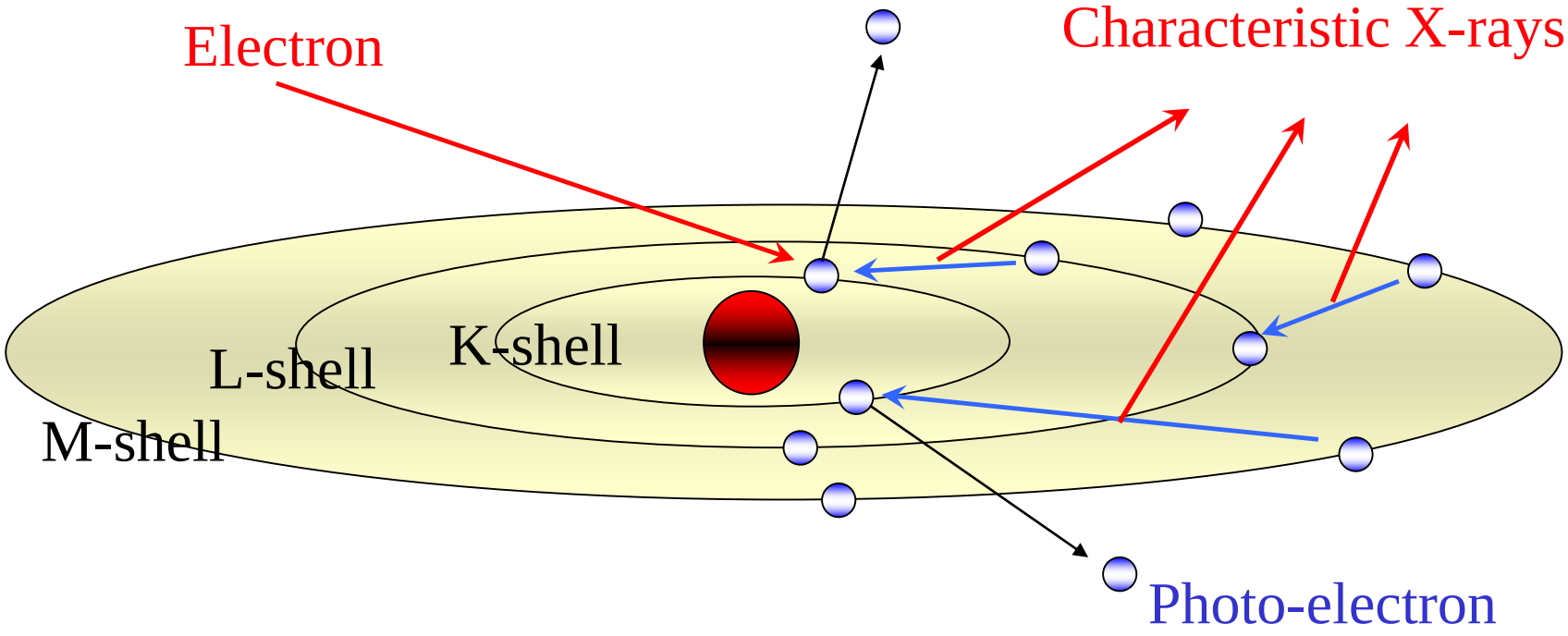
Electron
Characteristic X-rays
K-shell
L-shell
M-shell
Photo-electron

X-ray sources

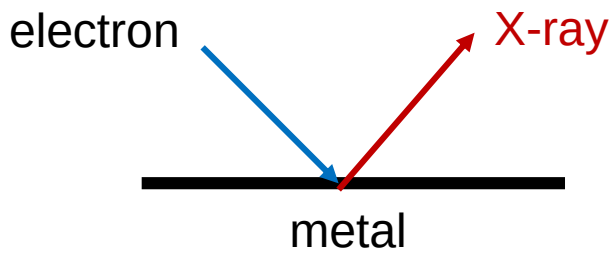

Mg K_α 1253.6 eV

Al K_α 1486.6 eV

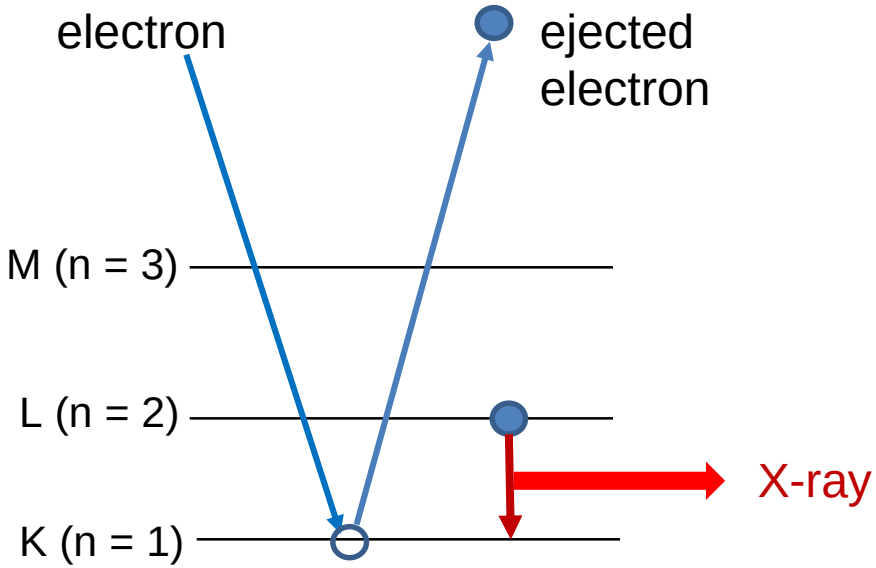

$L \rightarrow K : K_\alpha$

$M \rightarrow K : K_\beta$

$2P_{3/2} \rightarrow 1s : K_{\alpha 1}$

$2P_{1/2} \rightarrow 1s : K_{\alpha 2}$

X-ray absorption spectroscopy

XAS spectra are most often collected at **synchrotron** because of the high intensity of synchrotron X-ray sources

Absorption edge (energy that is just needed to eject a particular core electron, e.g., 1s e^- (K edge), $2p_{3/2}$ e^- (L_3 edge)
Fe K edge: 7.112 keV (λ = 0.174346 nm),
L_3 edge: 706.8 eV (λ = 1.7525 nm)

Within 10-40 eV: X-ray absorption near-edge structure (**XANES**) (or near Edge absorption fine structure (**NEXAFS**))
→ oxidation state & ligand environment

About 50 keV: extended X-ray absorption Fine structure (**EXAFS**)
→ distance & arrangement of atoms

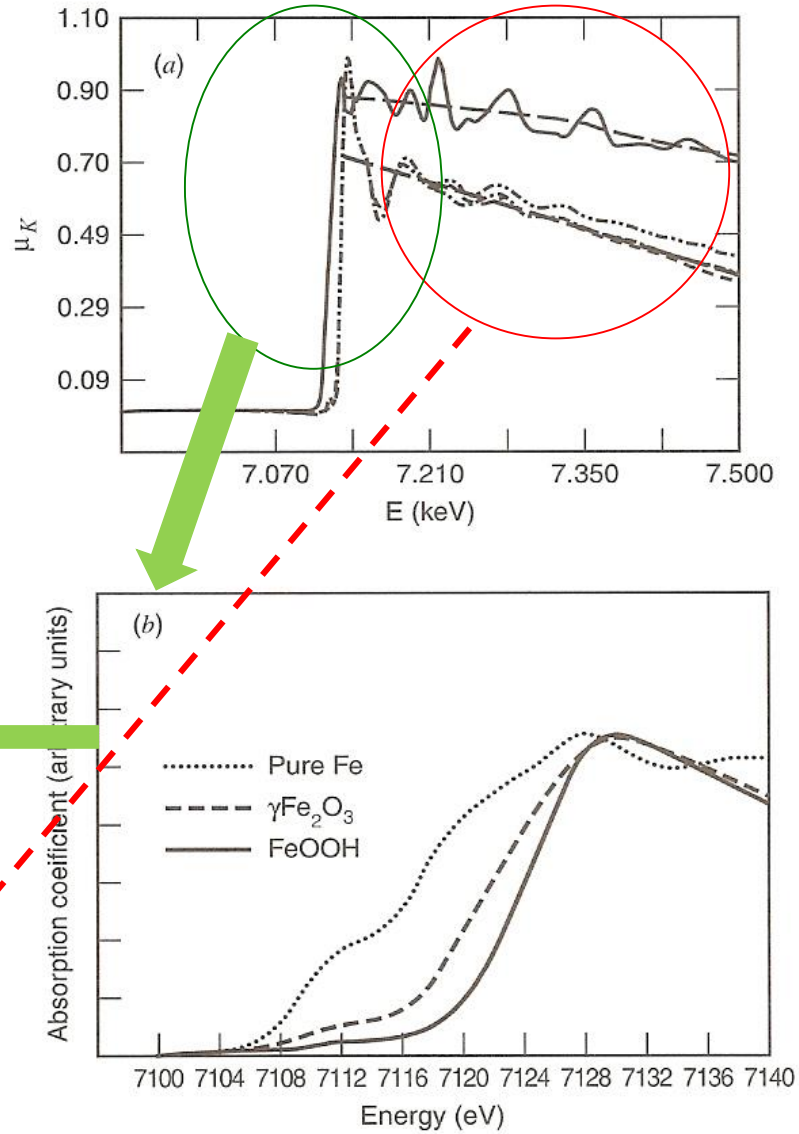

XAS techniques follow beer's law,

Transmitted X-ray intensity, $I_x = I_0 \exp(-\mu x)$

where μ: linear absorption coefficient

absorbance, $I_{abs} = I_0 - I_x$

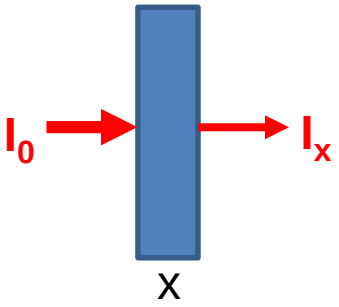

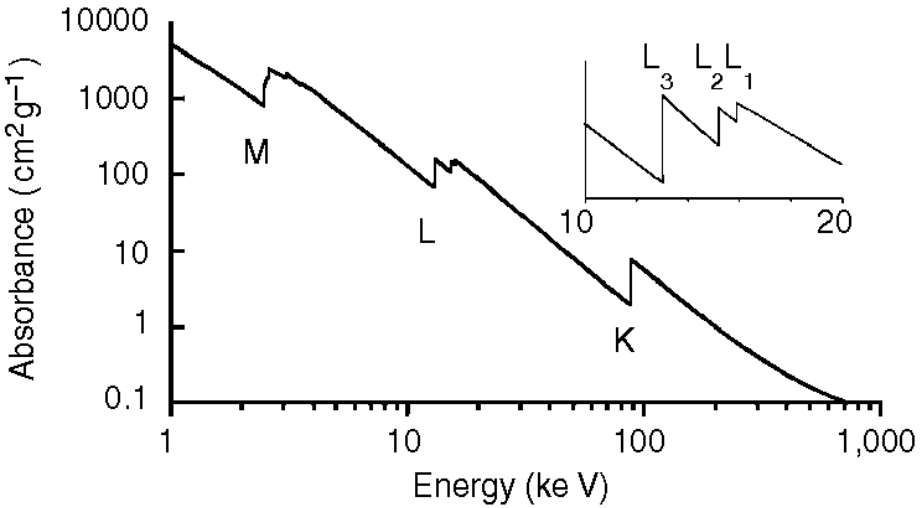

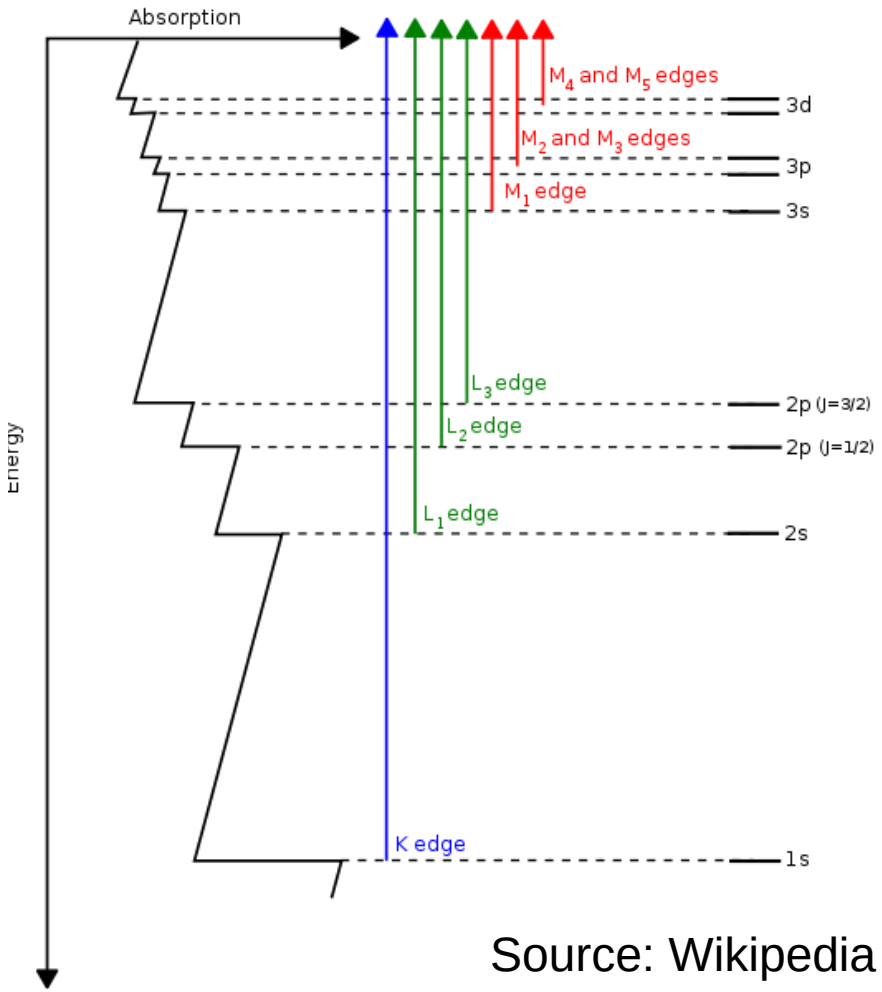

Source: Wikipedia

K (1s) and L_3 ($2p_{3/2}$) Electron Binding Energies for the Elements in Their Natural Forms, in eV

Legend: Element / K-edge / L_3-edge

H 13.6 n/a																	He 24.6 n/a
Li 54.7 n/a	Be 111.5 n/a											B 188 n/a	C 284.2 n/a	N 409.9 n/a	O 543.1 n/a	F 696.7 n/a	Ne 870.2 21.6
Na 1070.8 30.81	Mg 1303.0 49.50											Al 1559.6 72.55	Si 1839 99.42	P 2145.5 135	S 2472 162.5	Cl 2822 200	Ar 3205.9 248.5
K 3608.4 294.6	Ca 4038.5 346.2	Sc 4492 398.7	Ti 4966 453.8	V 5465 512.1	Cr 5989 574.1	Mn 6539 638.7	Fe 7112 706.8	Co 7709 778.1	Ni 8333 852.7	Cu 8979 932.7	Zn 9659 1021.8	Ga 10367 1116.4	Ge 11103 1217.0	As 11867 1323.6	Se 12658 1433.9	Br 13474 1550	Kr 14326 1678.4
Rb 15200 1804	Sr 16105 1940	Y 17038 2080	Zr 17998 2223	Nb 18986 2371	Mo 20000 2520	Tc 21044 2677	Ru 22117 2838	Rh 23220 3004	Pd 24350 3173	Ag 25514 3351	Cd 26711 3538	In 27940 3730	Sn 29200 3929	Sb 30491 4132	Te 31814 4341	I 33169 4557	Xe 34561 4786
Cs 35985 5012	Ba 37441 5247		Hf 65351 9561	Ta 67416 9881	W 69525 10207	Re 71676 10535	Os 73871 10871	Ir 76111 11215	Pt 78395 11546	Au 80725 11919	Hg 83102 12284	Tl 85530 12658	Pb 88005 13035	Bi 90524 13419	Po 93105 13814	At 95730 14214	Rn 98404 14619
Fr 101387 15031	Ra 103922 15444		Rf	Db	Sg	Bh	Hs	Mt	Ds	Rg	Cn	Uut	Uuq	Uup	Uuh	Uus	Uuo

La 38925 5483	Ce 40443 5723	Pr 41991 5964	Nd 43569 6208	Pm 45184 6459	Sm 46834 6716	Eu 48519 6977	Gd 50239 7243	Tb 51996 7514	Dy 53789 7790	Ho 55618 8071	Er 57486 8358	Tm 59390 8648	Yb 61332 8944	Lu 63314 9244
Ac 106768.2 15879.5	Th 109648.0 16300.0	Pa 112598.4 16732.9	U 115596.2 17164.7	Np 118688.7 17608.0	Pu 121790.2 18060.1	Am 124986.1 18510.0	Cm 128241.3 18970	Bk 131555.6 19449	Cf 134935.4 19901.2	Es 138391.5 20389.4	Fm 141930.4 20868.0	Md	No	Lr

J. A. Bearden and A. F. Burr, "Reevaluation of X-Ray Atomic Energy Levels," Rev. Mod. Phys. 39, 125 (1967)
M. Cardona and L. Ley, Eds., Photoemission in Solids I: General Principles (Springer-Verlag, Berlin, 1978)
J. C. Fuggle and N. Mårtensson, "Core-Level Binding Energies in Metals," J. Electron Spectrosc. Relat. Phenom. 21, 275 (1980)
Actinides (Ac-Fm): R.D. Deslattes, E.G. Kessler Jr., P. Indelicato, L. de Billy, E. Lindroth, J. Anton, J.S. Coursey, D.J. Schwab, J. Chang, R. Sukumar, K. Olsen, and R.A. Dragoset, "X-Ray Transition Energies Database", NIST Standard Reference Database 128, 2005; https://dx.doi.org/10.18434/T4859Z

When the incident x-ray energy matches the binding energy of an electron of an atom within the sample, the number of x-rays absorbed by the sample increases dramatically, causing a drop in the transmitted x-ray intensity. This results in an absorption edge. Every element has a set of unique absorption edges corresponding to different binding energies of its electrons, giving XAS element selectivity.

(1) XANES or NEXAFS

These spectra can be used to determine the average oxidation state of the element in the sample. The XANES spectra are also sensitive to the coordination environment of the absorbing atom in the sample.

Edge:
Oxidation state↑ → binding energy↑ → peak shift to higher energy

Electronegativity↑ → binding energy↑ → peak shift to higher energy

Pre-edge: not dipole transition rule ($\Delta l = \pm 1$), but $\Delta l = \pm 2$ (ex : 1s→3d) → low intensity

Geometry of metal ion on p-d orbital mixing

bonding distance on p-d orbital mixing

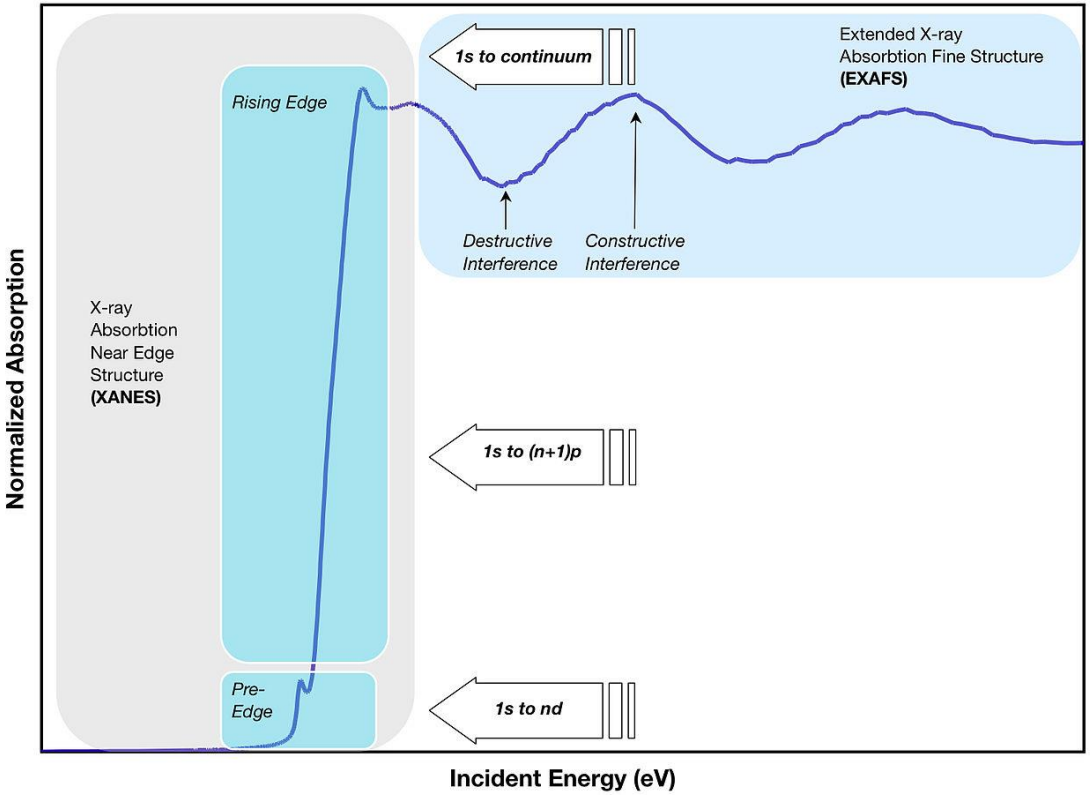

Source: Wikipedia

e.g. oxygen reduction reaction

$Co_{0.25}Mn_{0.75}Fe_{2.0}O_4$

half-wave potential of 0.904 V (versus RHE) & mass activity of 46.9 A g_{oxide}^{-1} (at 0.9 V vs RHE) with promising stability

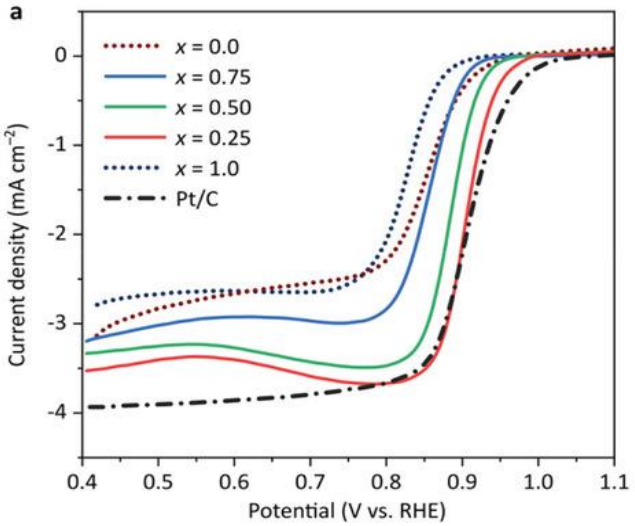

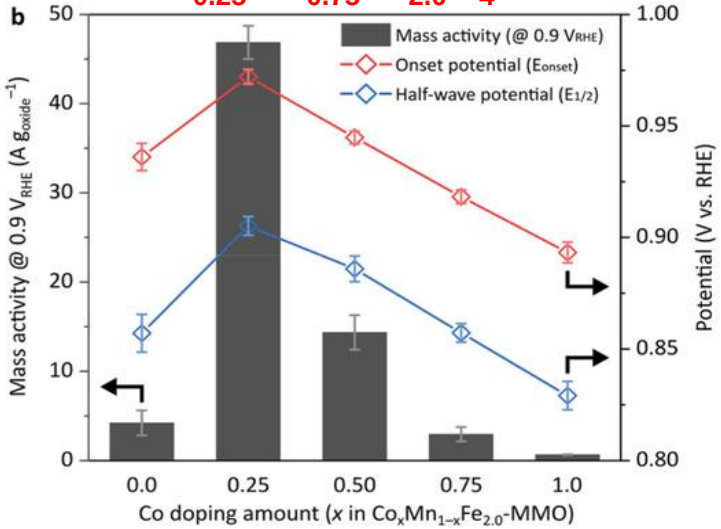

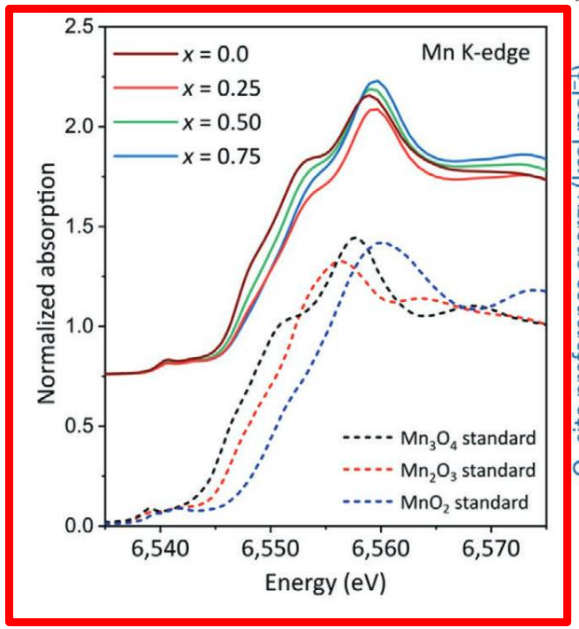

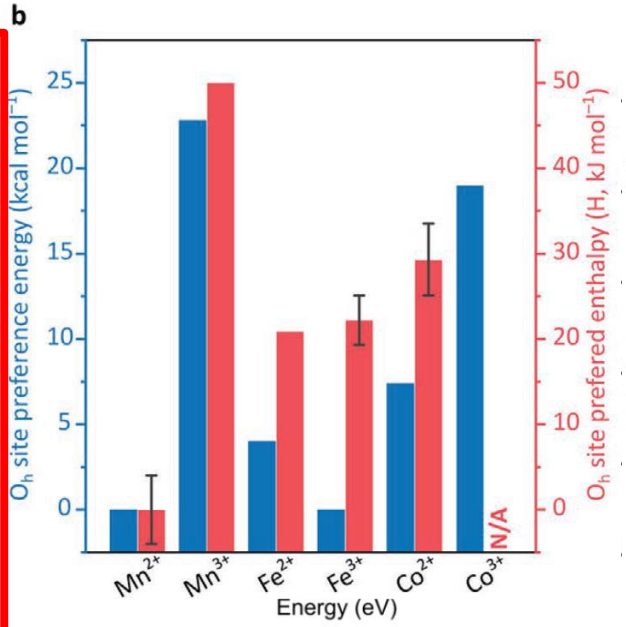

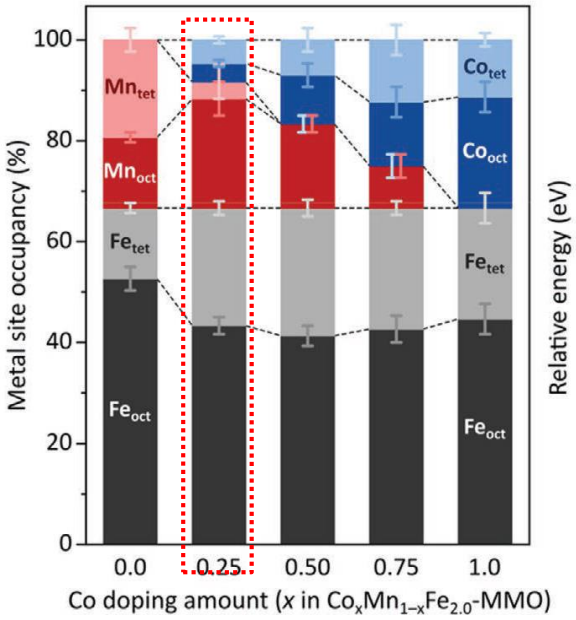

✓ XANES spectra show an increase in the Mn oxidation state, whereas the Fe and Co cations maintain oxidation states according to Co doping amounts ($\mathbf{Co_xMn_{1-x}Fe_{2.0}O_4}$)

Adv. Mater. **2022**, *34*, 2107868.

(2) EXAFS

The ejected photoelectron interacts with electrons in the surrounding non-excited atoms. If the ejected photoelectron is taken to have a wave-like nature and the surrounding atoms are described as point scatters, it is possible to imagine the backscattered electron waves interfering with the forward-propagating waves. The resulting interference pattern shows up as a modulation of the measured absorption coefficient, thereby causing the oscillation in the EXAFS spectra. The dependence of the scattering on atomic species makes it possible to obtain information pertaining to the chemical coordination environment of the original absorbing (centrally excited) atom by analyzing these EXAFS data.

Source: Wikipedia

e.g. synthesis & characterization of electrocatalysts

Co 1.4 wt%

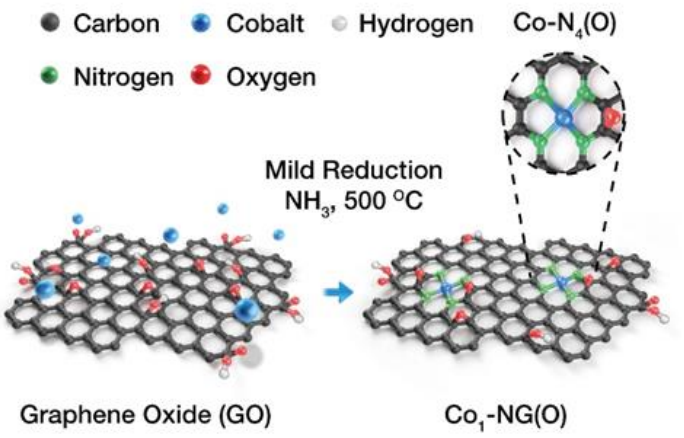

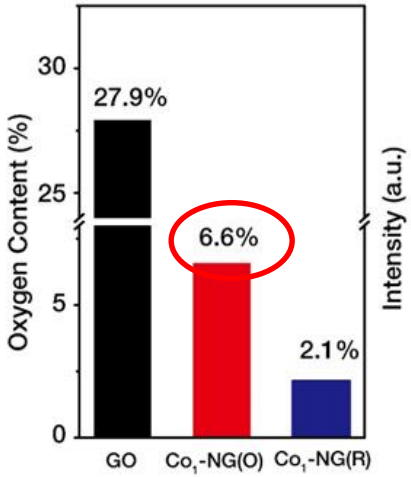

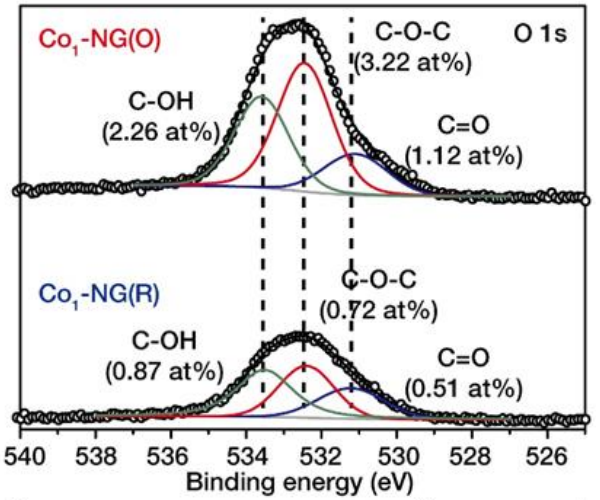

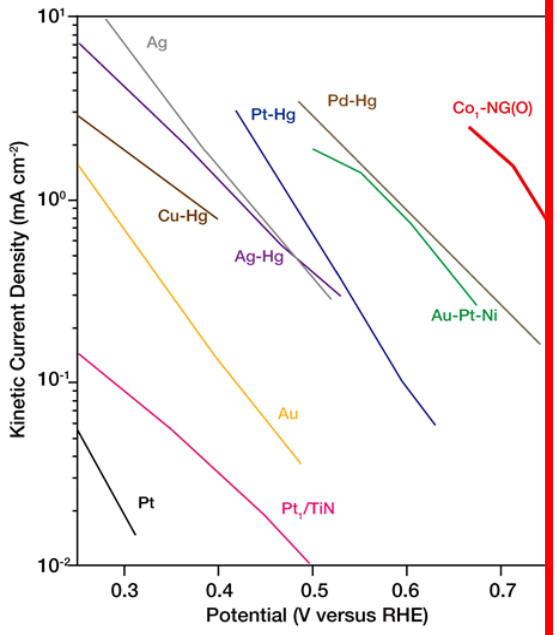

H_2O_2 production

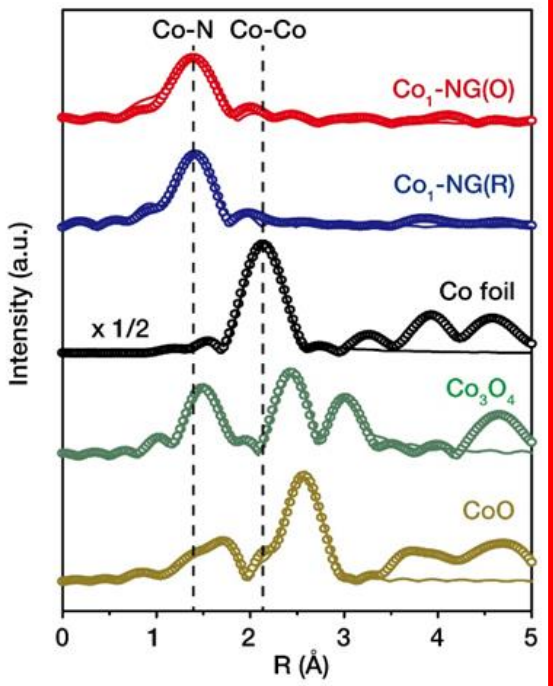

EXAFS: no Co-Co peak

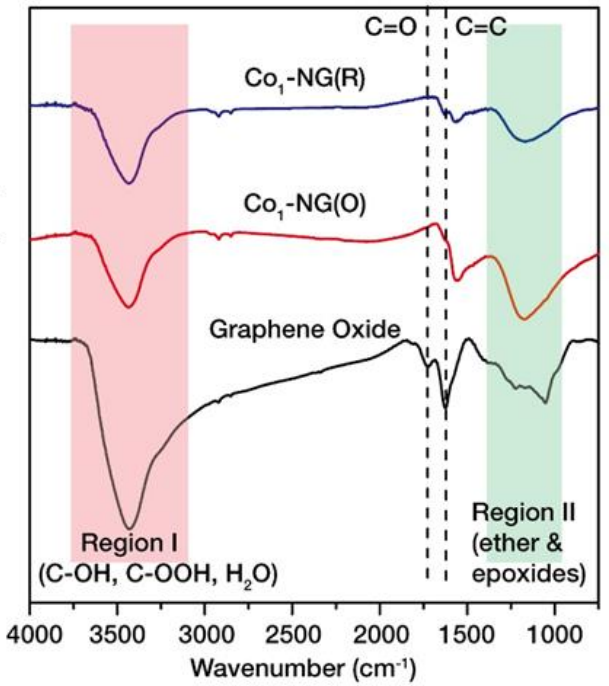

Nature Materials. 19 (2020) 436

Electron source

Ultra high vacuum (UHV)

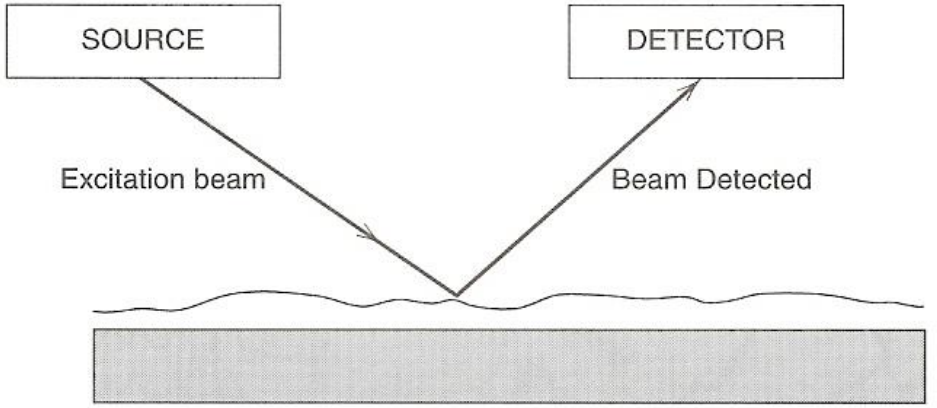

	Excitation	Detection
X-ray photoelectron spectroscopy (XPS)	Photons(X-ray)	Electrons
UV photoelectron spectroscopy (UPS)	Photons (UV)	Electrons
Auger electron spectroscopy (AES)	Electrons	Electrons
Low-energy electron diffraction (LEED)	Electrons	Electrons
High resolution e^- E loss spec. (HREELS)	Electrons	Electrons
Rutherford backscattering (RBS)	H+ or He+	H+ or He+
Secondary ion mass spec. (SIMS)	Ions	Ions
Laser desorption mass spec. (LDMS)	Photons	Ions

Electron diffraction

LEED(low energy, 10~200 eV): surface & adsorbate structure

TEM(transmission, 60~300 keV, SAED): crystal structure

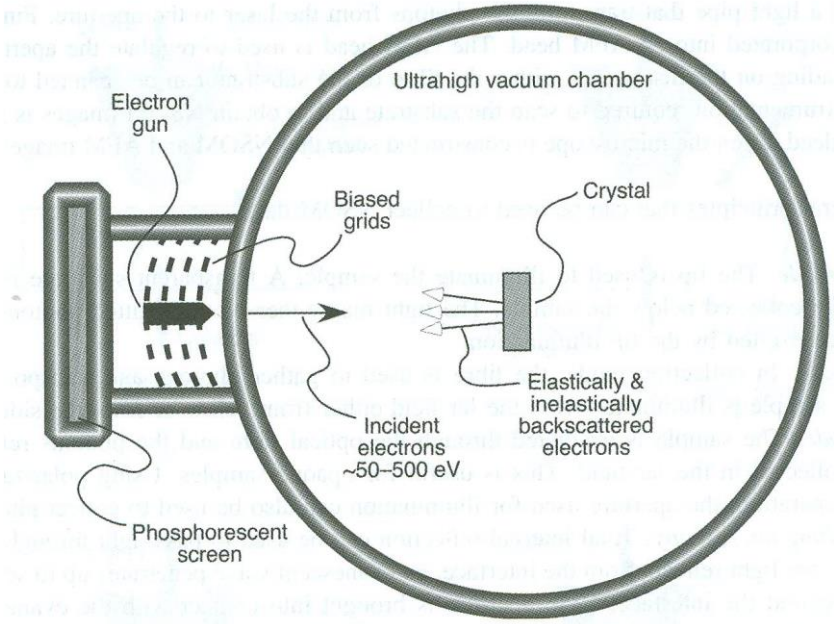

Figure 2.12 Schematic drawing of a LEED chamber.

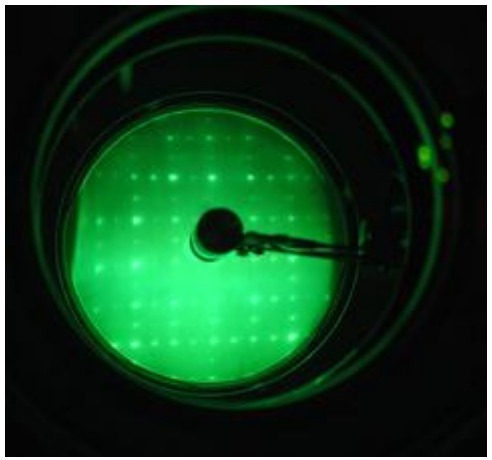

Si(100), LEED

en.wikipedia.org

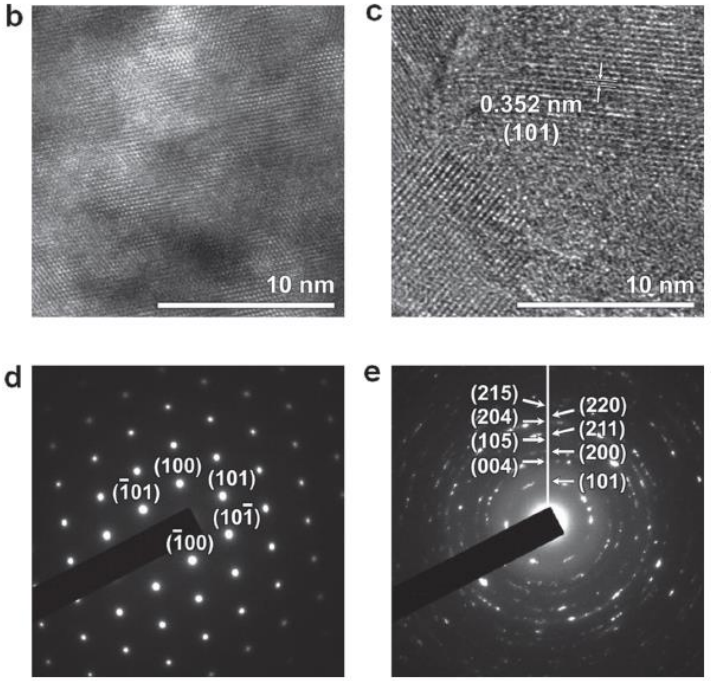

TEM & SAED(Selected Area Electron Diffraction)

Small (2017)

Surface diffraction

- Low energy electron diffraction (LEED), X-ray diffraction, atomic diffraction

de Broglie wavelength, λ, of a particle $\lambda = h/p$

$$\lambda = \frac{h}{\sqrt{2mE}} \tag{2.1}$$

where h is Planck's constant, m is the mass of the particle, and E is the kinetic energy of the particle. For electrons and He atoms, Eq. 2.1 is more conveniently expressed as:

$$\lambda_{e^-}\,(\text{Å}) = \sqrt{\frac{150}{E\,(\text{eV})}} \quad \text{and} \quad \lambda_{He}\,(\text{Å}) = \sqrt{\frac{0.02}{E\,(\text{eV})}} \tag{2.2}$$

For X-rays, the wavelength of a photon is given by

$$\lambda_{photon}\,(\text{Å}) \approx \frac{1.24 \times 10^4}{E\,(\text{eV})} \tag{2.3}$$

Electrons with 10~200 eV energies and He atoms with thermal energies (~0.026 eV at 300K) → atomic diffraction condition (λ < interatomic distance, ~1 Å)

X-rays at the high intensities available at a synchrotron radiation suitable for surface and interface structure studies (grazing angle X-ray diffraction). X-ray bombardment-induced emission of electrons also shows diffraction (photoelectron diffraction)

LEED: electron beam of 10~200 eV is back-scattered → atomic structure of surface

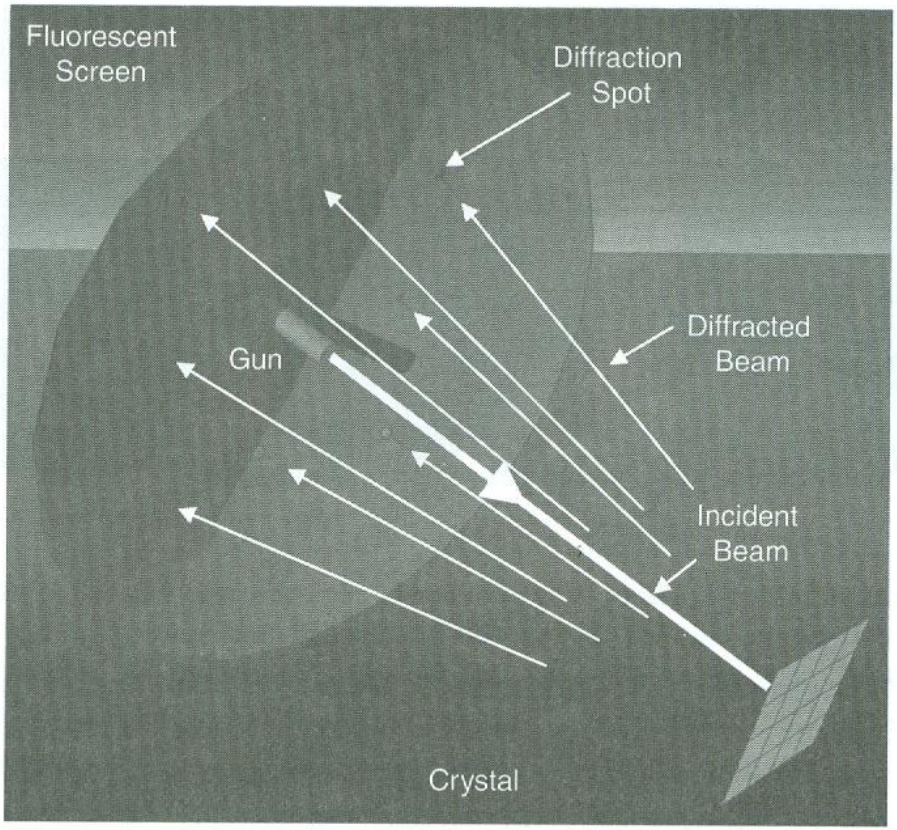

Figure 2.7. A scheme illustration of LEED surface crystallography.

Low energy electron diffraction (LEED):

Why low energy electron used?

- The penetration depth of X-ray is ~ 1 μm. So X-ray diffraction give structural information of a bulk solid (3D). It does not have any surface sensitivity
- The penetration depth of low energy electron is ≤ 20 Å; a rather good surface sensitivity
- In any diffraction the employed wavelength λ should ~ d

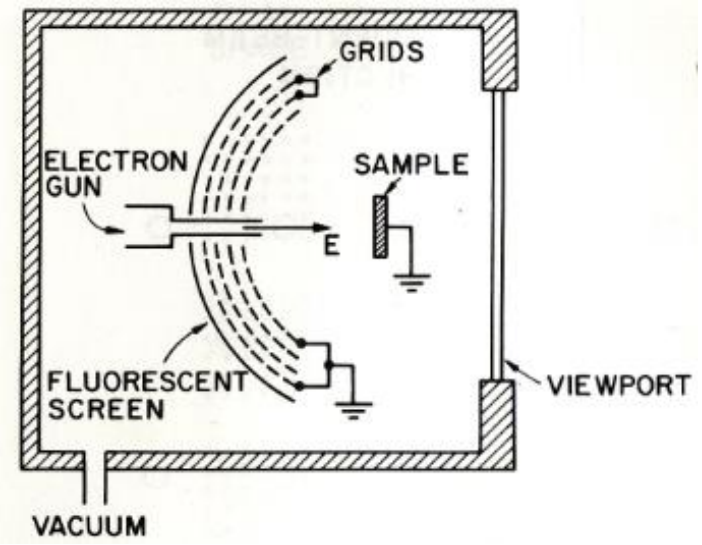

- De Broglie wavelength of $\mathbf{e}^-$ is

$$\lambda = h/p = h/ mv = h/(2mE_k)^{1/2}$$

If E_k= 150 eV, λ =~ 1 Å

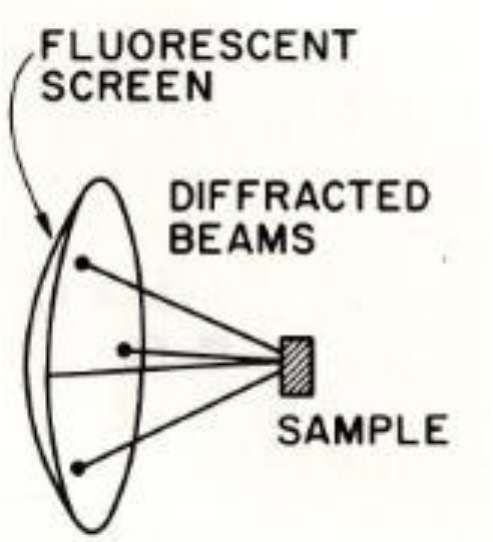

- Since diffraction can be observed in elastic scattering,
  the inelastically scattered electrons have to be removed by setting up an potential barrier (grid assembly)

Reciprocal lattice

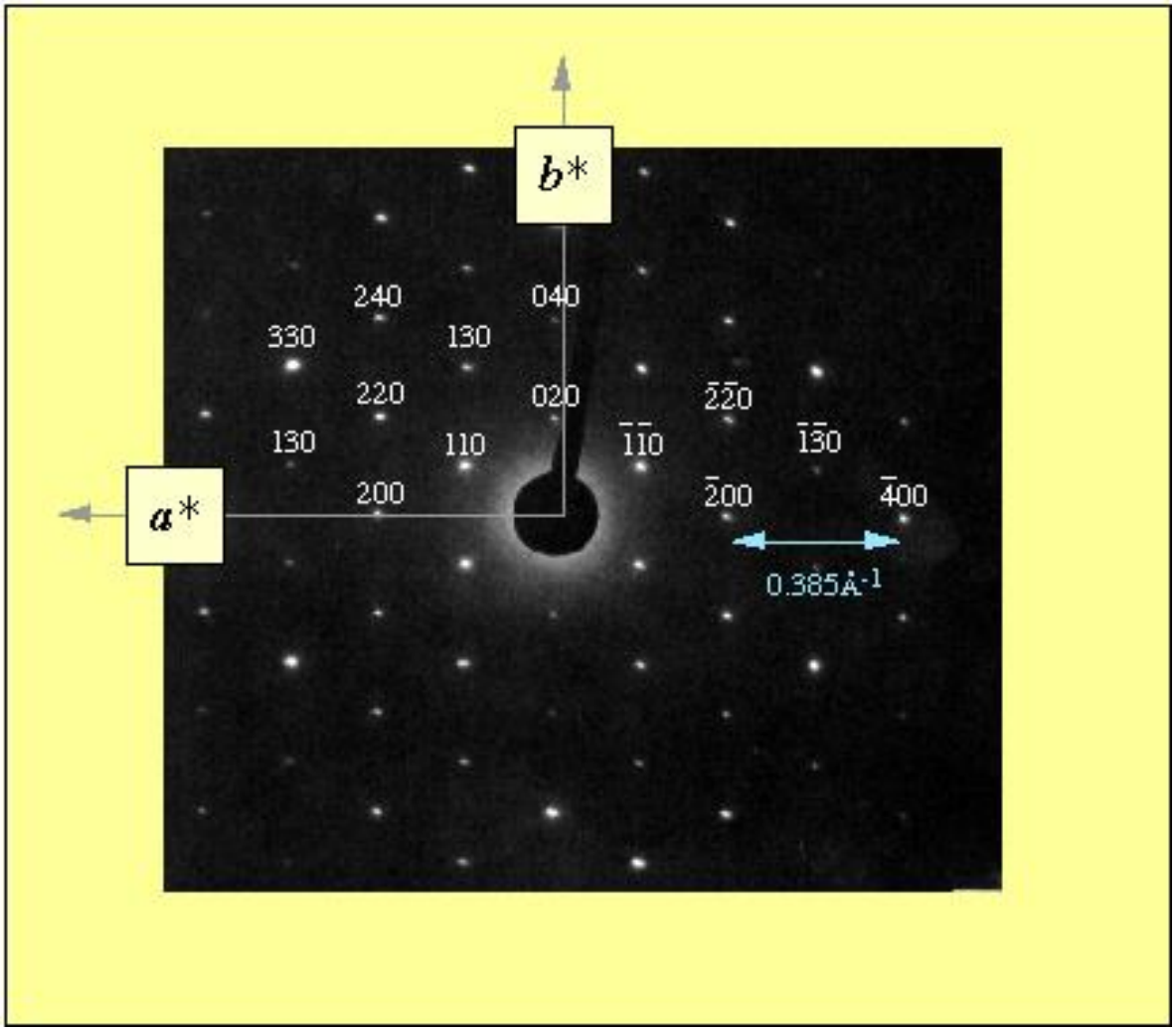

clay.uga.edu

3-D

real unit vector $\vec{a}_1, \vec{a}_2, \vec{a}_3$

reciprocal vector $\vec{a}_1^*, \vec{a}_2^*, \vec{a}_3^*$

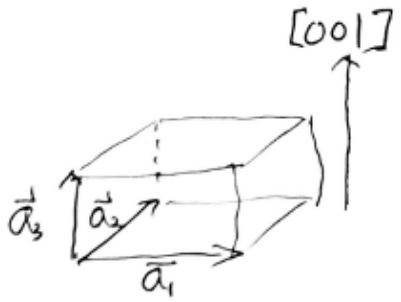

Volume, $V = \vec{a}_3 \cdot (\vec{a}_1 \times \vec{a}_2) = \vec{a}_1 \cdot (\vec{a}_2 \times \vec{a}_3) = \vec{a}_2 \cdot (\vec{a}_3 \times \vec{a}_1)$

$\vec{a}_1^* = \frac{1}{V}(\vec{a}_2 \times \vec{a}_3)$, $\vec{a}_2^* = \frac{1}{V}(\vec{a}_3 \times \vec{a}_1)$, $\vec{a}_3^* = \frac{1}{V}(\vec{a}_1 \times \vec{a}_2)$

$|\vec{a}_3^*| = \frac{|\vec{a}_1 \times \vec{a}_2|}{V} = \frac{1}{d_{001}}$ d plane

$|\vec{a}_1^*| = \frac{1}{d_{100}}$, $|\vec{a}_2^*| = \frac{1}{d_{010}}$

reciprocal lattice vector

$$\vec{g}_{hkl} = h\vec{a}_1^* + k\vec{a}_2^* + l\vec{a}_3^*$$

$$|\vec{g}_{hkl}| = \frac{1}{d_{hkl}}, \quad \vec{g}_{hkl} \perp (hkl)$$

$$\vec{a}_i \cdot \vec{a}_j^* = 1 \ (i=j), \quad \vec{a}_i \cdot \vec{a}_j^* = 0 \ (i \neq j)$$

Further note:

Ewald sphere: reciprocal lattice illustrating the Laue(Bragg) conditions

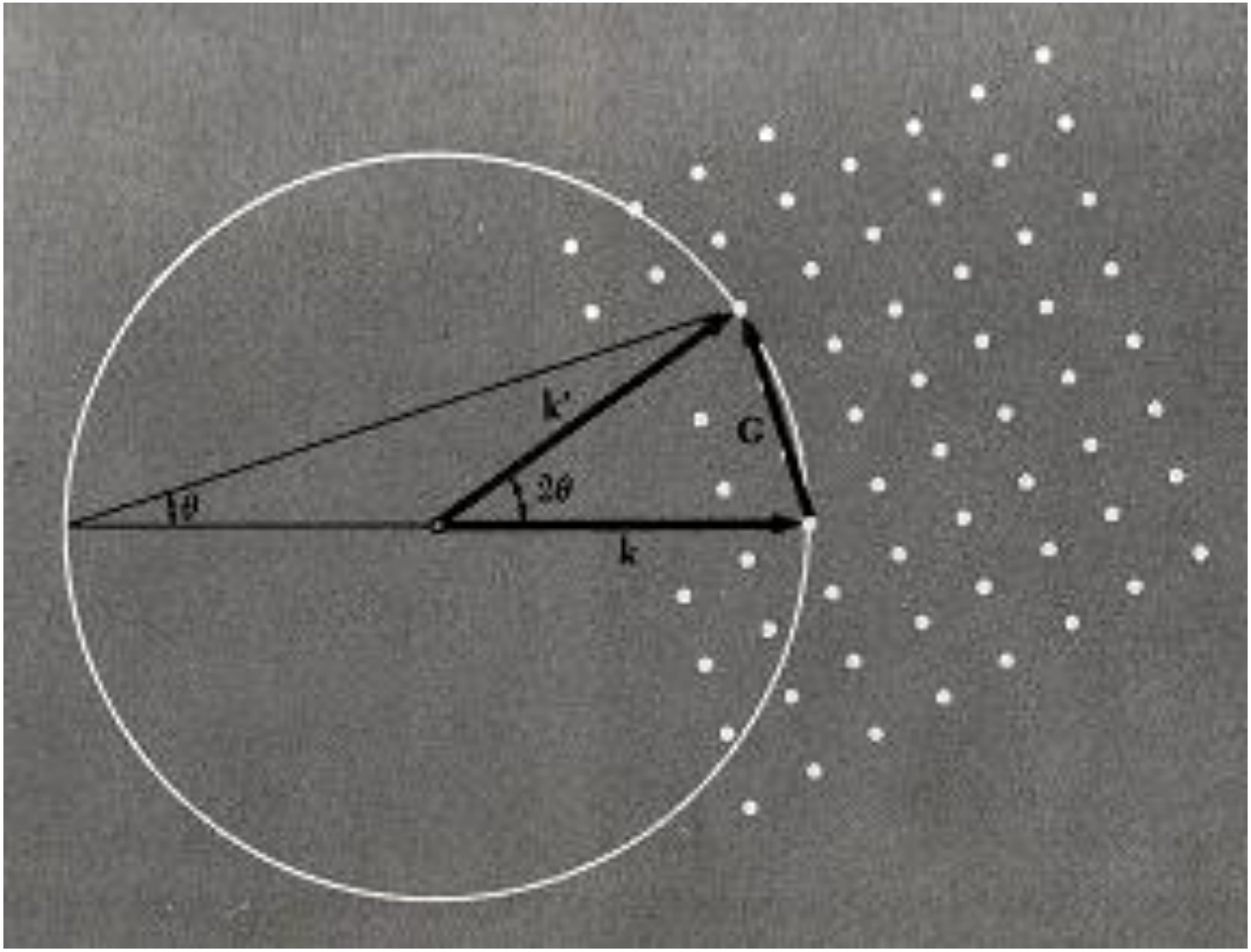

TEM → SAED (selected area electron diffraction)

- selected area, $\theta = 0 \sim 2°$ (very small θ)
- 60 ~ 300 keV electron beam

  e.g. 100 keV → $\lambda = 3.88$ pm (very small)

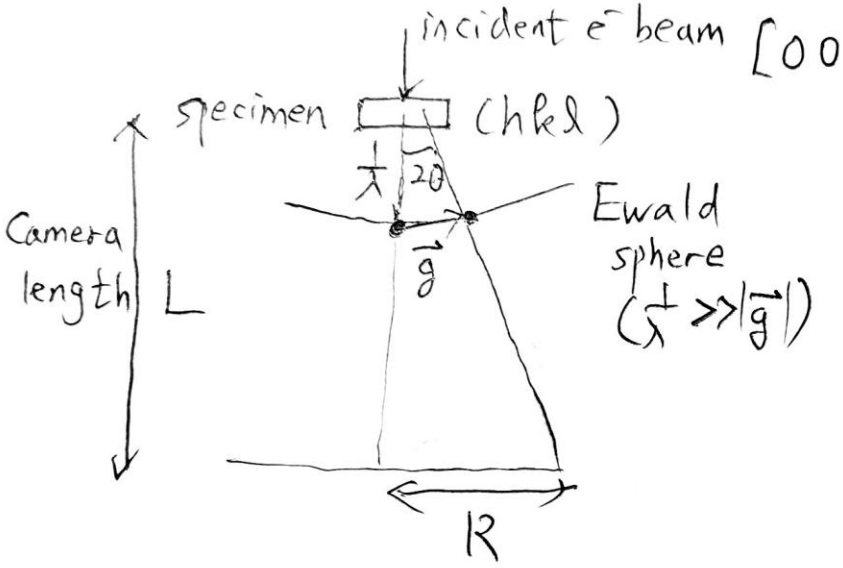

$\lambda = 2d\sin\theta$

$= 2d\theta$, $g = \frac{1}{d}$

$\frac{1}{\lambda} : g = L : R$

$\Rightarrow \lambda L = \frac{R}{g} = R \cdot d$

$\vec{g} = k_D - k_i$ (diffracted − incident)

$|\vec{g}| = \frac{1}{d_{hkl}}$

$\frac{1}{\lambda} >> \vec{g}$

Reciprocal lattice (2-D)

Basis vectors $\mathbf{a_1}$, $\mathbf{a_2}$ in the unit cell in real space
Basis vectors $\mathbf{a_1}^*$, $\mathbf{a_2}^*$ in a reciprocal space

The real and reciprocal space lattices are represented by

$$\mathbf{a}_i \cdot \mathbf{a}_j^* = \delta_{ij} \tag{2.5.5}$$

where $i, j = 1$ or 2 and δ_{ij} is the Kronecker δ function. $\delta_{ij} = 0$ if $i \neq j$ and $\delta_{ij} = 1$ if $i = j$. This means that $\mathbf{a}_i^* \perp \mathbf{a}_j$ for $i \neq j$. Introducing γ and γ^*, which are the angles between ($\mathbf{a_1}$ and $\mathbf{a_2}$) and ($\mathbf{a_1}^*$ and $\mathbf{a_2}^*$), respectively, the relationships between these angles and the lengths of the basis vectors are

$$a_1^* = 1/(a_1 \sin\gamma) \tag{2.5.6}$$

$$a_2^* = 1/(a_2 \sin\gamma) \tag{2.5.7}$$

$$\sin\gamma = \sin\gamma^*. \tag{2.5.8}$$

The inverse relationship between real and reciprocal space means that a long vector in real space corresponds to a short vector in reciprocal space. Eq. (2.5.8) follows from the relationship $\gamma^* = \pi - \gamma$.

The need for the reciprocal space description is made evident by Figure 2.14. This figure shows that an image of the diffracted electrons corresponds to a reciprocal space image of the lattice from which the electrons diffracted. Hence, by uncovering the relationship between a reciprocal space image and the real space lattice, we can use LEED patterns to investigate the surface structure.

Reciprocal lattice

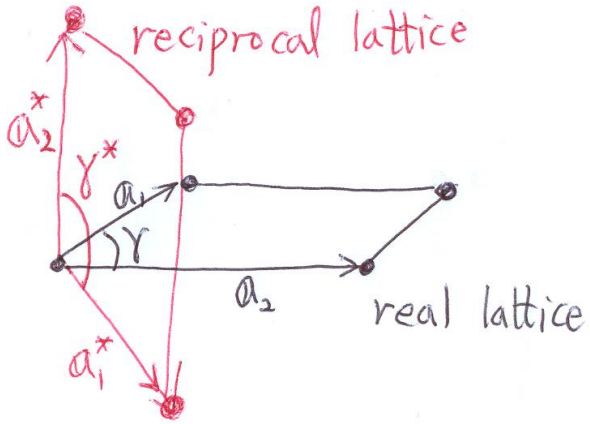

A: real lattice → unit cell

A^*: reciprocal lattice → unit cell

$$A = |a_1 \times a_2| = a_1 a_2 \sin\gamma$$

$$A^* = |a_1^* \times a_2^*| = a_1^* a_2^* \sin\gamma^* = \frac{1}{A}$$

$$(\sin\gamma = \sin\gamma^*)$$

$$A A^* = (a_1 a_1^* \sin\gamma)(a_2 a_2^* \sin\gamma) = 1$$

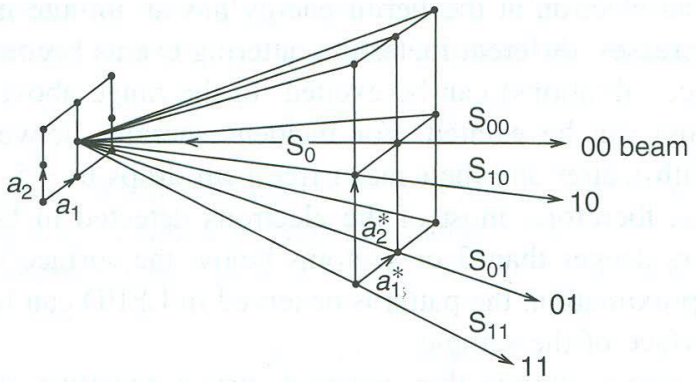

Figure 2.14 *The principle of diffraction pattern formation in a LEED experiment. The incident electron beam approaches along s_0. The specular beam exits along s_{00}. Reproduced from G. Ertl, J. Küppers,* Low Energy Electrons and Surface Chemistry, *2nd ed., VCH, Weinheim. © 1985, with permission from John Wiley & Sons, Ltd.*

The diffraction condition from a one-dimensional lattice of periodicity a leads to constructive interference at angles φ when

$$a \sin \varphi = n\lambda \qquad (2.5.18)$$

Bragg's law

for an electron with a wavelength λ incident at normal incidence. n is an integer denoting the diffraction order. The wavelength of the electron is given by the de Broglie relationship, Eq. (2.4.9). The Bragg condition of Eq. (2.5.18) needs to be generalized to two dimensions. This leads to the Laue conditions

$$\mathbf{a_1} \cdot (\mathbf{s} - \mathbf{s_0}) = h_1 \lambda \qquad (2.5.19)$$

$$\mathbf{a_2} \cdot (\mathbf{s} - \mathbf{s_0}) = h_2 \lambda \qquad (2.5.20)$$

Laue conditions

where $\mathbf{s_0}$ defines the direction of the incident beam (generally along the surface normal) and $\mathbf{s}$ defines the direction of the diffracted beam intensity maxima. h_1 and h_2 are integers. They are used to identify the diffraction reflexes that appear in the LEED pattern. The specular reflex at (00) is used as the origin and arises from electrons that are elastically scattered without diffraction.

Further note:

Brillouin zone: perpendicular bisectors of reciprocal lattice vectors

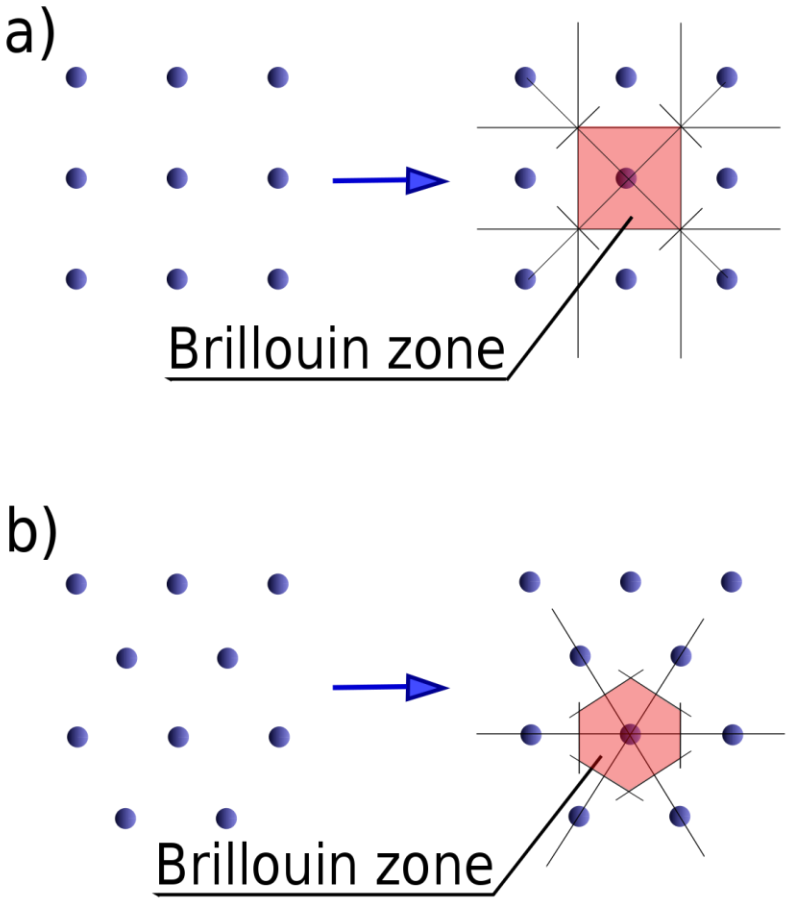

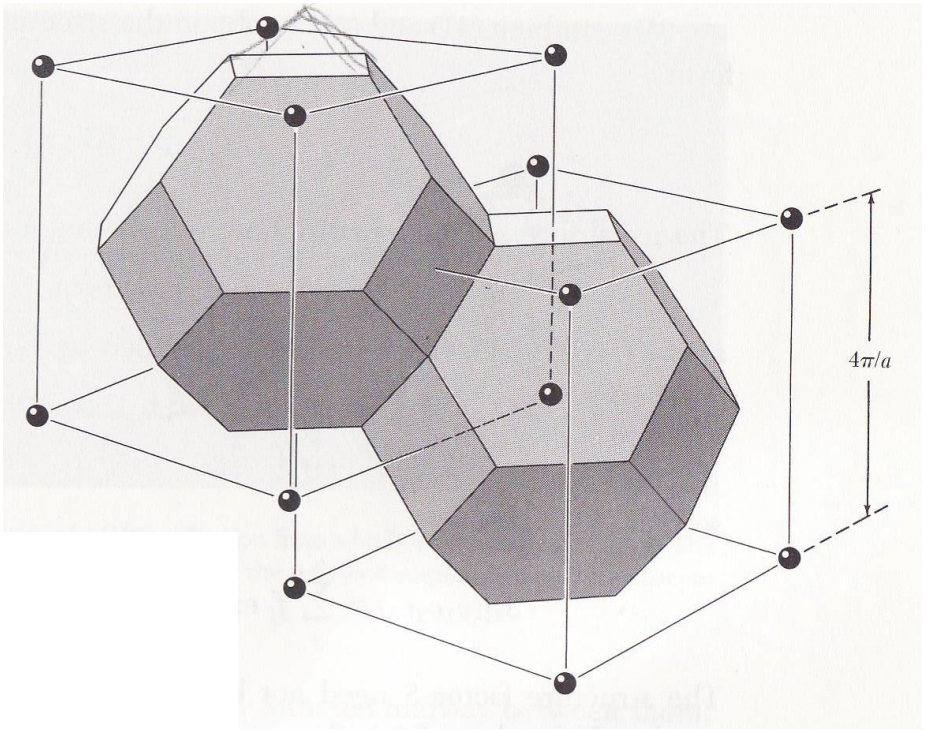

Matrix notation for adsorbate

$$b_1 = m_{11} a_1 + m_{12} a_2$$

$$b_2 = m_{21} a_1 + m_{22} a_1$$

in matrix notation, $\quad b = \mathfrak{M} \cdot a \qquad \mathfrak{M} = \begin{pmatrix} m_{11} & m_{12} \\ m_{21} & m_{22} \end{pmatrix}$

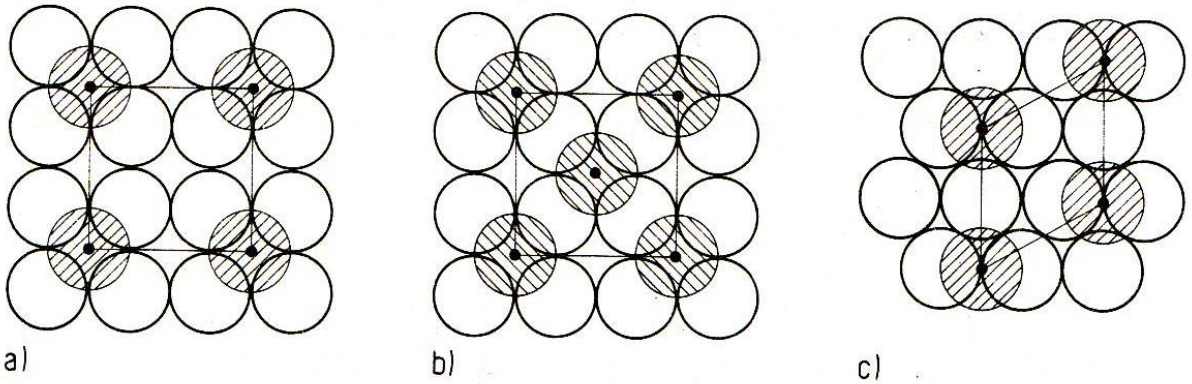

Fig. 9.2. Examples for overlayer structures. a) 2×2, b) $c(2 \times 2)$, c) $\sqrt{3} \times \sqrt{3}/\mathrm{R}\ 30°$.

$$\mathfrak{M} = \begin{pmatrix} 2 & 0 \\ 0 & 2 \end{pmatrix}, \begin{pmatrix} 1 & 1 \\ -1 & 1 \end{pmatrix} \text{ and } \begin{pmatrix} 1 & 1 \\ -1 & 2 \end{pmatrix}$$

2D real vs. reciprocal lattices of adsorbate

$$b_1 = m_{11}a_1 + m_{12}a_2 \qquad b_1^* = m_{11}^* a_1^* + m_{12}^* a_2^*$$
$$b_2 = m_{21}a_1 + m_{22}a_2 \,. \qquad b_2^* = m_{21}^* a_1^* + m_{22}^* a_2^* \,.$$

$\mathfrak{M}^* = \tilde{\mathfrak{M}}^{-1}$, and so $\mathfrak{M} = \tilde{\mathfrak{M}}^{*-1}$

m*: inverse transposed matrix of m

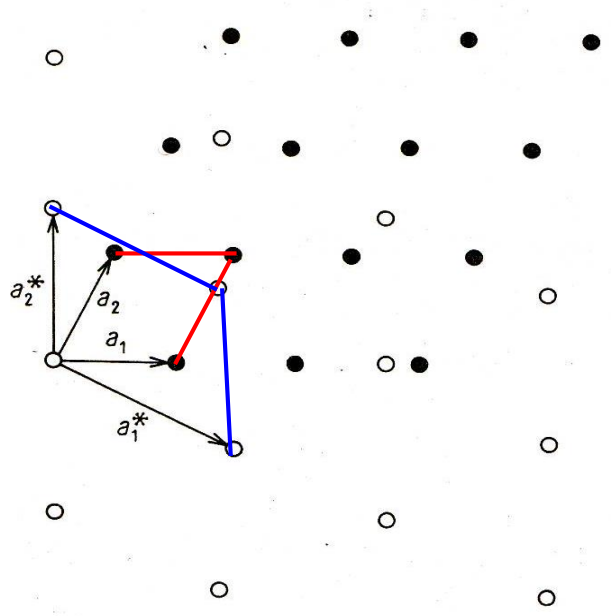

Fig. 9.11. A two-dimensional real lattice, described by a_1, a_2 (dark circles), and its reciprocal lattice a_1^*, a_2^* (open circles).

$$m_{11} = \frac{1}{\det \mathfrak{M}^*} \cdot m_{22}^*$$

$$m_{12} = -\frac{1}{\det \mathfrak{M}^*} \cdot m_{21}^*$$

$$m_{21} = -\frac{1}{\det \mathfrak{M}^*} \cdot m_{12}^*$$

$$m_{22} = \frac{1}{\det \mathfrak{M}^*} \cdot m_{11}^*$$

where det **M*** = $m_{11}^* \cdot m_{22}^* - m_{21}^* \cdot m_{12}^*$

m_{ij}^* can be measured directly from LEED pattern → Target: m_{ij} can be calculated from reciprocal pattern

real $|b = |M \cdot a \Rightarrow \begin{pmatrix} |b_1 \\ |b_2 \end{pmatrix} = \overset{|M}{\begin{pmatrix} m_{11} & m_{12} \\ m_{21} & m_{22} \end{pmatrix}} \begin{pmatrix} a_1 \\ a_2 \end{pmatrix}$

reciprocal $|b^* = |M^* \cdot a^* \Rightarrow \begin{pmatrix} |b_1^* \\ |b_2^* \end{pmatrix} = \overset{|M^*}{\begin{pmatrix} m_{11}^* & m_{12}^* \\ m_{21}^* & m_{22}^* \end{pmatrix}} \begin{pmatrix} a_1^* \\ a_2^* \end{pmatrix}$

cf. Inverse matrix : $A = \begin{bmatrix} a & b \\ c & d \end{bmatrix} \Rightarrow A^{-1} = \frac{1}{ad-bc} \begin{bmatrix} d & -b \\ -c & a \end{bmatrix}$, $ad-bc$: determinant of A

transposed matrix : $A = \begin{bmatrix} a & b \\ c & d \end{bmatrix} \Rightarrow \widehat{A} = \begin{bmatrix} a & c \\ b & d \end{bmatrix}$

inverse matrix $|M^{-1} = \frac{1}{\det |M^*} \begin{pmatrix} m_{22}^* & -m_{12}^* \\ -m_{21}^* & m_{11}^* \end{pmatrix}$, $|M^{*-1} = \frac{1}{\det M} \begin{pmatrix} m_{22} & -m_{12} \\ -m_{21} & m_{11} \end{pmatrix}$

inversed transposed matrix

$\widetilde{M}^{-1} = \frac{1}{\det |M^*} \begin{pmatrix} m_{22}^* & -m_{21}^* \\ -m_{12}^* & m_{11}^* \end{pmatrix}$, $\widetilde{|M}^{*-1} = \frac{1}{\det M} \begin{pmatrix} m_{22} & -m_{21} \\ -m_{12} & m_{11} \end{pmatrix}$

$$\boxed{|M = \widetilde{|M}^{*-1}}$$

$\mathfrak{M}^* = \overline{\mathfrak{M}}^{-1}$, and so $\mathfrak{M} = \overline{\mathfrak{M}}^{*-1}$

$$\boldsymbol{b}_1 = m_{11}\boldsymbol{a}_1 + m_{12}\boldsymbol{a}_2 \qquad \boldsymbol{b}_1^* = m_{11}^*\boldsymbol{a}_1^* + m_{12}^*\boldsymbol{a}_2^*$$
$$\boldsymbol{b}_2 = m_{21}\boldsymbol{a}_1 + m_{22}\boldsymbol{a}_2 . \qquad \boldsymbol{b}_2^* = m_{21}^*\boldsymbol{a}_1^* + m_{22}^*\boldsymbol{a}_2^* .$$

$\boldsymbol{b}_i \cdot \boldsymbol{b}_j = \delta_{ij}$ $\quad \delta_{ij} = 0$ if $i \neq j$

$\boldsymbol{a}_i \cdot \boldsymbol{a}_j = \delta_{ij}$ $\quad \delta_{ij} = 1$ if $i = j$

$\Rightarrow$ prove $M^* \overline{M} = 1$

$$\begin{pmatrix} m_{11}^* & m_{12}^* \\ m_{21}^* & m_{22}^* \end{pmatrix} \begin{pmatrix} m_{11} & m_{21} \\ m_{12} & m_{22} \end{pmatrix} = \begin{pmatrix} m_{11}^* m_{11} + m_{12}^* m_{12} & m_{11}^* m_{21} + m_{12}^* m_{22} \\ m_{21}^* m_{11} + m_{22}^* m_{12} & m_{21}^* m_{21} + m_{22}^* m_{22} \end{pmatrix} = \begin{pmatrix} 1 & 0 \\ 0 & 1 \end{pmatrix}$$

$1 = \boldsymbol{b}_1 \cdot \boldsymbol{b}_1^* = (m_{11}\boldsymbol{a}_1 + m_{12}\boldsymbol{a}_2)(m_{11}^*\boldsymbol{a}_1^* + m_{12}^*\boldsymbol{a}_2^*) = m_{11}m_{11}^* + m_{12}m_{12}^*$ $\quad (\because \boldsymbol{a}_1 \cdot \boldsymbol{a}_1^* = \boldsymbol{a}_2 \cdot \boldsymbol{a}_2^* = 1,\ \boldsymbol{a}_1 \cdot \boldsymbol{a}_2^* = \boldsymbol{a}_2 \cdot \boldsymbol{a}_1^* = 0)$

$0 = \boldsymbol{b}_1 \cdot \boldsymbol{b}_2^* = (\quad)(\quad) = m_{11}^* m_{21} + m_{12}^* m_{22}$

$0 = \boldsymbol{b}_2 \cdot \boldsymbol{b}_1^* = (\quad)(\quad) = m_{21}^* m_{11} + m_{22}^* m_{12}$

$1 = \boldsymbol{b}_2 \cdot \boldsymbol{b}_2^* = (\quad)(\quad) = m_{21}^* m_{21} + m_{22}^* m_{22}$

//

We represent a surface overlayer by the basis vectors $\mathbf{b_1}$ and $\mathbf{b_2}$ and the corresponding reciprocal lattice vectors are given stars. The substrate and overlayer lattices are related by

$$\mathbf{b_1} = m_{11}\mathbf{a_1} + m_{12}\mathbf{a_2} \tag{2.5.9}$$

$$\mathbf{b_2} = m_{21}\mathbf{a_1} + m_{22}\mathbf{a_2} \tag{2.5.10}$$

$$\mathbf{b_1^*} = m_{11}^*\mathbf{a_1^*} + m_{12}^*\mathbf{a_2^*} \tag{2.5.11}$$

$$\mathbf{b_2^*} = m_{21}^*\mathbf{a_1^*} + m_{22}^*\mathbf{a_2^*}. \tag{2.5.12}$$

This can be written in matrix notation as

$$\mathbf{b} = \mathbf{M}\cdot\mathbf{a} \rightarrow \begin{pmatrix}\mathbf{b}_1\\ \mathbf{b}_2\end{pmatrix} = \begin{pmatrix}m_{11} & m_{12}\\ m_{21} & m_{22}\end{pmatrix}\cdot\begin{pmatrix}\mathbf{a}_1\\ \mathbf{a}_2\end{pmatrix}. \tag{2.5.13}$$

A similar relationship holds for the reciprocal space representation

$$\mathbf{b}^* = \mathbf{M}^*\cdot\mathbf{a}^* \rightarrow \begin{pmatrix}\mathbf{b}_1^*\\ \mathbf{b}_2^*\end{pmatrix} = \begin{pmatrix}m_{11}^* & m_{12}^*\\ m_{21}^* & m_{22}^*\end{pmatrix}\cdot\begin{pmatrix}\mathbf{a}_1^*\\ \mathbf{a}_2^*\end{pmatrix}. \tag{2.5.14}$$

It can be shown that **M*** is related to **M** (and vice versa) by

$$\mathbf{M} = \frac{1}{\det\mathbf{M}^*}\begin{pmatrix}m_{22}^* & -m_{21}^*\\ -m_{12}^* & m_{11}^*\end{pmatrix} \tag{2.5.15}$$

$$\mathbf{M}^* = \frac{1}{\det\mathbf{M}}\begin{pmatrix}m_{22} & -m_{21}\\ -m_{12} & m_{11}\end{pmatrix} \tag{2.5.16}$$

The determinant of **M*** is define as

$$\det\mathbf{M}^* = m_{11}^*\,m_{22}^* - m_{21}^*\,m_{12}^*, \tag{2.5.17}$$

and analogously for the determinant of **M**. Experimentally, the challenge is to determine the elements of **M** from the diffraction pattern measured on the LEED screen.

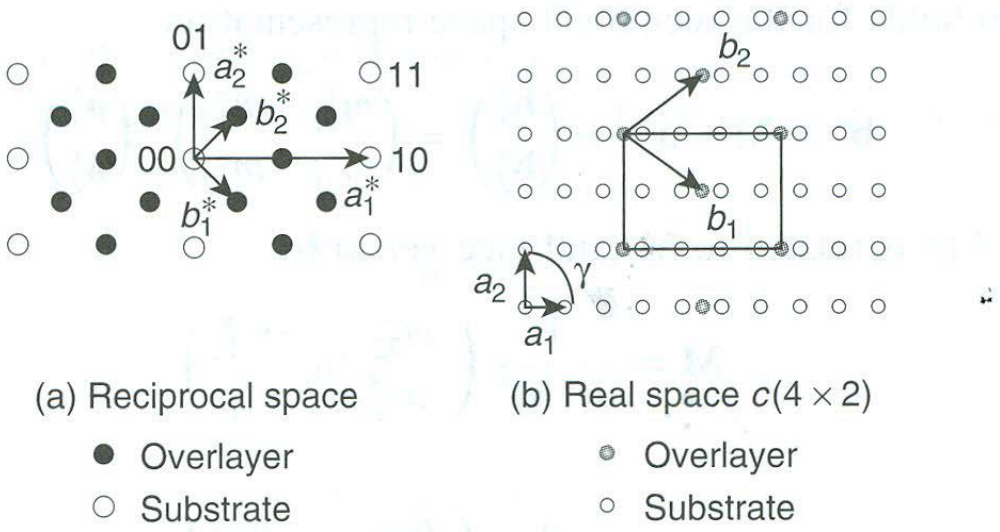

Figure 2.15 *Real space and reciprocal space patterns. (a) Reciprocal lattice (LEED pattern) composed o substrate (normal) spots ○ and overlayer (extra) spots ●. (b) Real lattice of the substrate (○) and overlayer (◉) The solid line delineates the c(4 × 2) cell and the arrows depict the unit vectors.*

From (a)

i) $\mathbf{b}_1^* = \frac{1}{4}\mathbf{a}_1^* - \frac{1}{2}\mathbf{a}_2^* = m_{11}^*\mathbf{a}_1^* + m_{12}^*\mathbf{a}_2^*$

$\mathbf{b}_2^* = \frac{1}{4}\mathbf{a}_1^* + \frac{1}{2}\mathbf{a}_2^* = m_{21}^*\mathbf{a}_1^* + m_{22}^*\mathbf{a}_2^*$

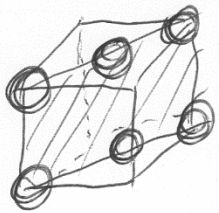

fcc(110)

ii) $\mathbf{a}_1 \perp \mathbf{a}_2^*$, $\mathbf{a}_2 \perp \mathbf{a}_1^*$

Substrate → position area

$a_1 = \frac{1}{a_1^* \sin\gamma} = \frac{1}{a_1^*}$, $a_2 = \frac{1}{a_2^* \sin\gamma} = \frac{1}{a_2^*} = \frac{\sqrt{2}}{a_1^*} = \sqrt{2}\,a_1$

$(\gamma = 90^\circ)$

iii) $\mathbf{b}_1^*, \mathbf{b}_2^* \longrightarrow \mathbf{b}_1, \mathbf{b}_2$, $\det|M^*| = \begin{vmatrix} \frac{1}{4} & -\frac{1}{2} \\ \frac{1}{4} & \frac{1}{2} \end{vmatrix} = \frac{1}{4}$

adsorbate

$m_{11} = \frac{m_{22}^*}{\det|M^*|} = \frac{1}{2}\Big/\left(\frac{1}{4}\right) = 2$, $m_{12} = \frac{-m_{21}^*}{\det|M^*|} = -1$, $m_{21} = \frac{-m_{12}^*}{\det|M^*|} = 2$, $m_{22} = 1$

$|M| = \begin{pmatrix} 2 & -1 \\ 2 & 1 \end{pmatrix}$ $\therefore \mathbf{b}_1 = 2\mathbf{a}_1 - \mathbf{a}_2$

$\mathbf{b}_2 = 2\mathbf{a}_1 + \mathbf{a}_2$ (Fig 2.15(b))

LEED image

Bisulfate/Pt(111)

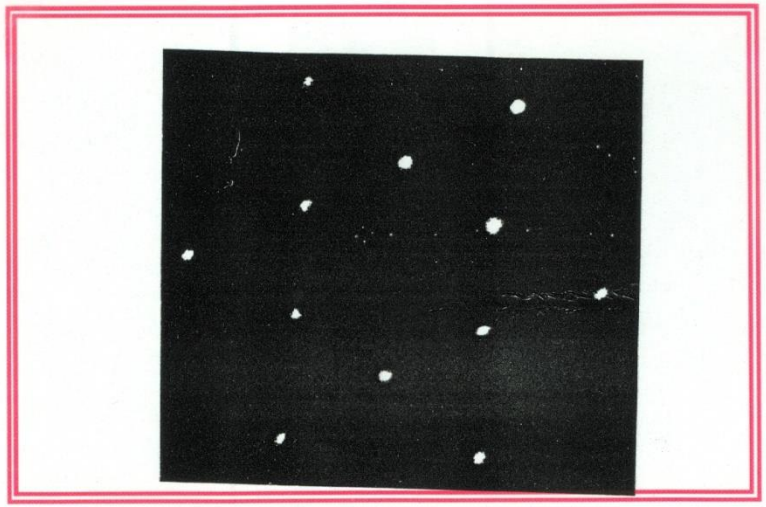

E = 0.34 V in 50 mM sulfuric acid 49.4 eV

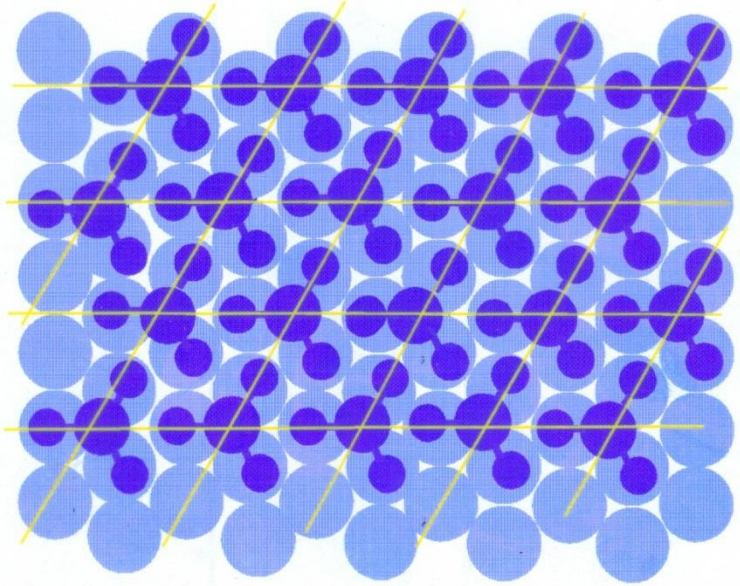

$(\sqrt{3} \times \sqrt{3})R30^\circ$

Sung's Ph.D thesis

Spectroscopic surface methods

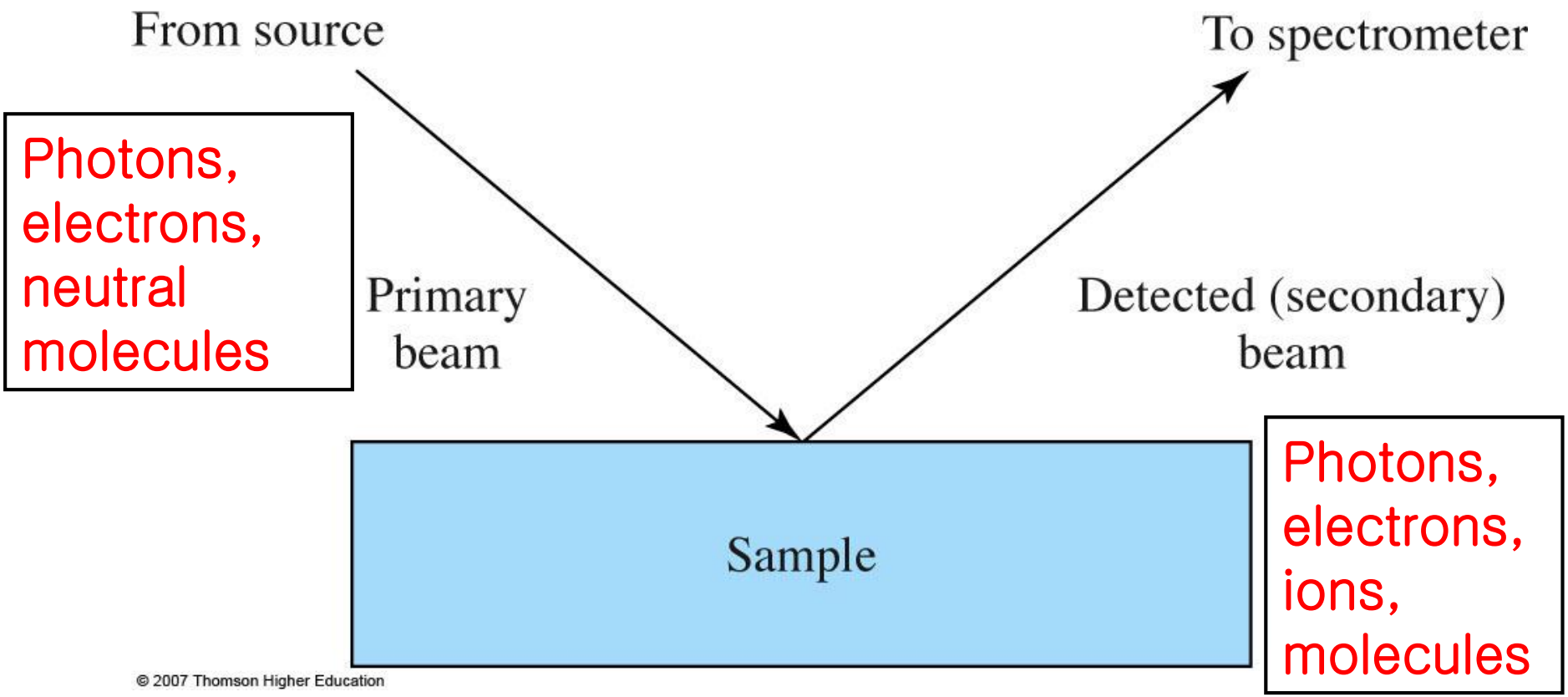

Atomic lamps: H (10.2 eV)
He (21.1, 42.82 eV) → UV sources, UPS
Xe lamp (170~3000 nm)

Skoog, Holler, Crouch, *Principles of Instrumental Analysis* (Thomson)

TABLE 21-1 Some Common Spectroscopic Techniques for Analysis of Surfaces

Method and Acronym	Primary Beam	Detected Beam	Information
X-ray photoelectron spectroscopy (XPS), or electron spectroscopy for chemical analysis (ESCA)	X-ray photons	Electrons	Chemical composition Chemical structure
Auger electron spectroscopy (AES)	Electrons or X-ray photons	Electrons	Chemical composition
Electron energy-loss spectroscopy (EELS)	Electrons	Electrons	Chemical structure Adsorbate binding
Electron microprobe (EM)	Electrons	X-ray photons	Chemical composition
Secondary-ion mass spectrometry (SIMS)	Ions	Ions	Chemical composition Chemical structure
Ion-scattering spectroscopy (ISS) and Rutherford backscattering	Ions	Ions	Chemical composition Atomic structure
Laser-microprobe mass spectrometry (LMMS)	Photons	Ions	Chemical composition Chemical structure
Surface plasmon resonance (SPR)	Photons	Photons	Composition and concentration of thin films
Sum frequency generation (SFG)	Photons	Photons	Interface structure, adsorbate binding
Ellipsometry	Photons	Photons	Thin-film thickness

Skoog, Holler, Crouch, *Principles of Instrumental Analysis* (Thomson)

Electron spectroscopy

XPS (X-ray photoelectron spectroscopy)
UPS (UV photoelectron spectroscopy)
AES (Auger electron spectroscopy)

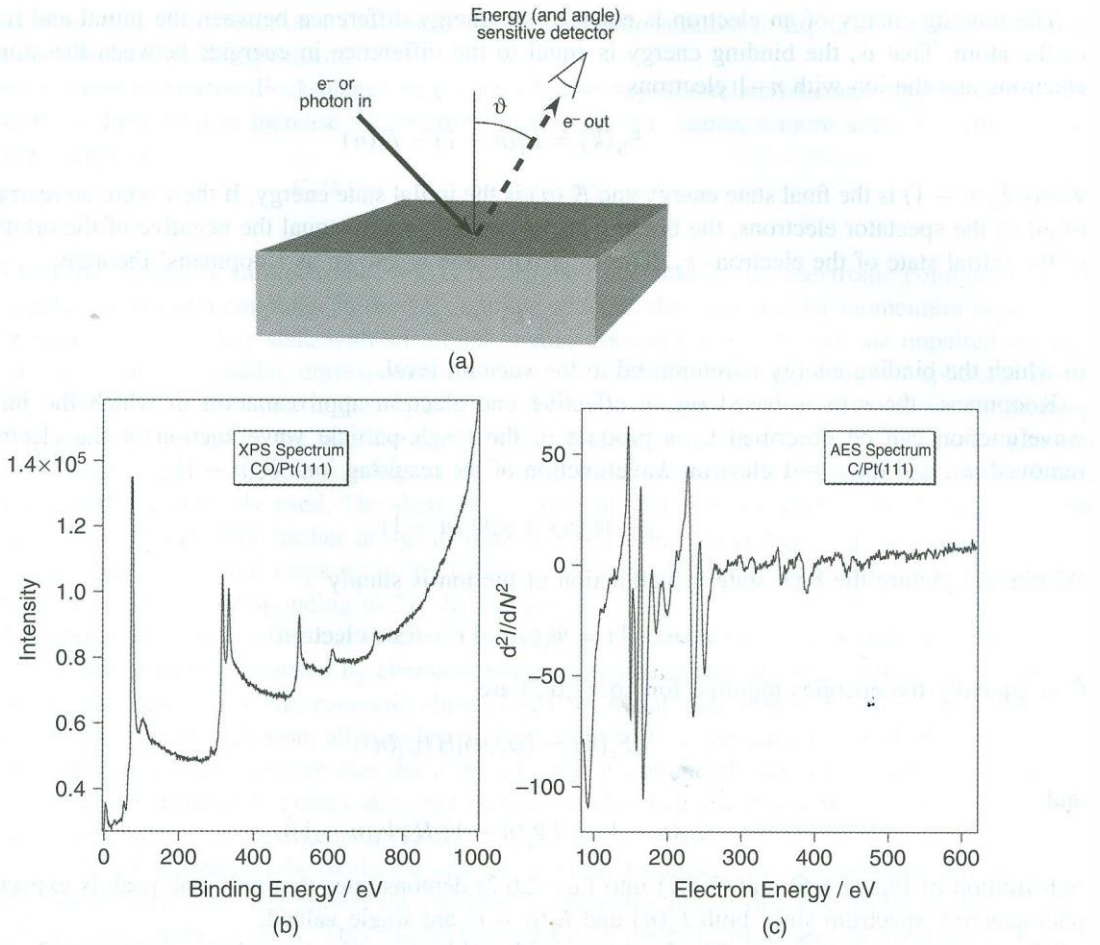

Figure 2.17 *(a) Schematic representation of electron spectroscopy. (b) A sample XPS spectrum of CO/Pt(111). (c) A sample AES spectrum of CO/Pt(111).*

X-ray photoelectron spectroscopy (XPS) or electron spectroscopy for chemical analysis (ESCA)

Binding energy of core electron ~ photon energy of X-ray region

$$E_b = h\nu - E_k - w \qquad (21\text{-}2)$$

w: work function of spectrometer

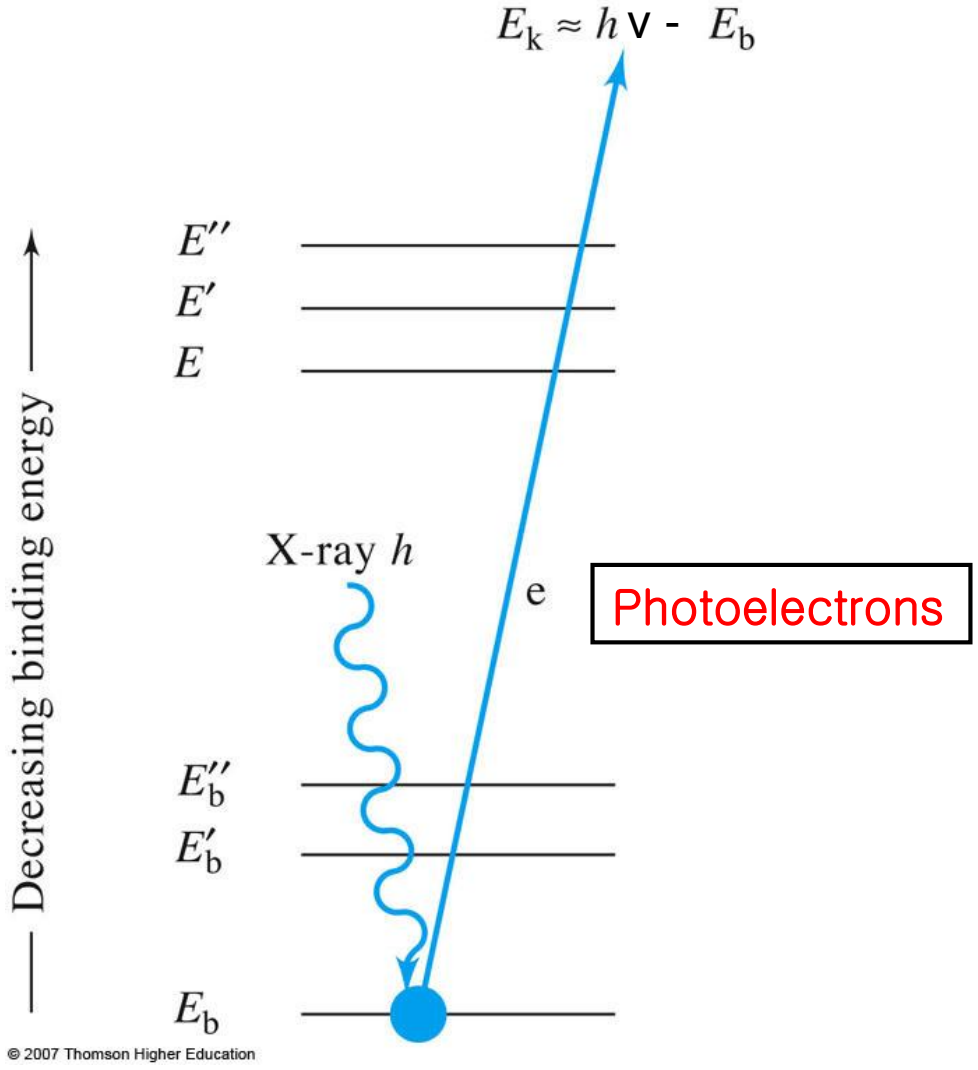

Skoog, Holler, Crouch, Principles of Instrumental Analysis (Thomson)

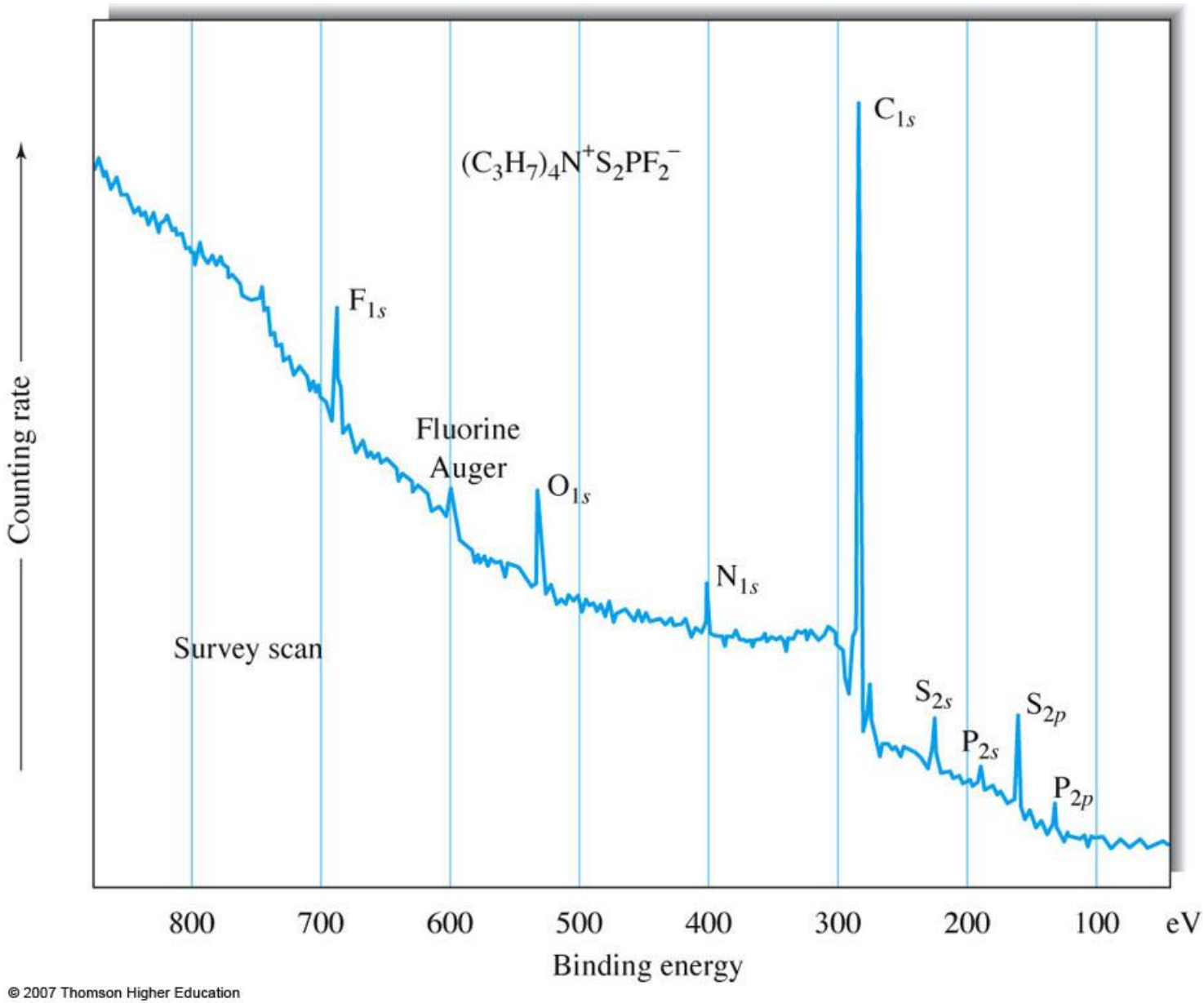

Skoog, Holler, Crouch, Principles of Instrumental Analysis (Thomson)

Environmental effect by electronegativity

electronegativity↑→ binding energy↑

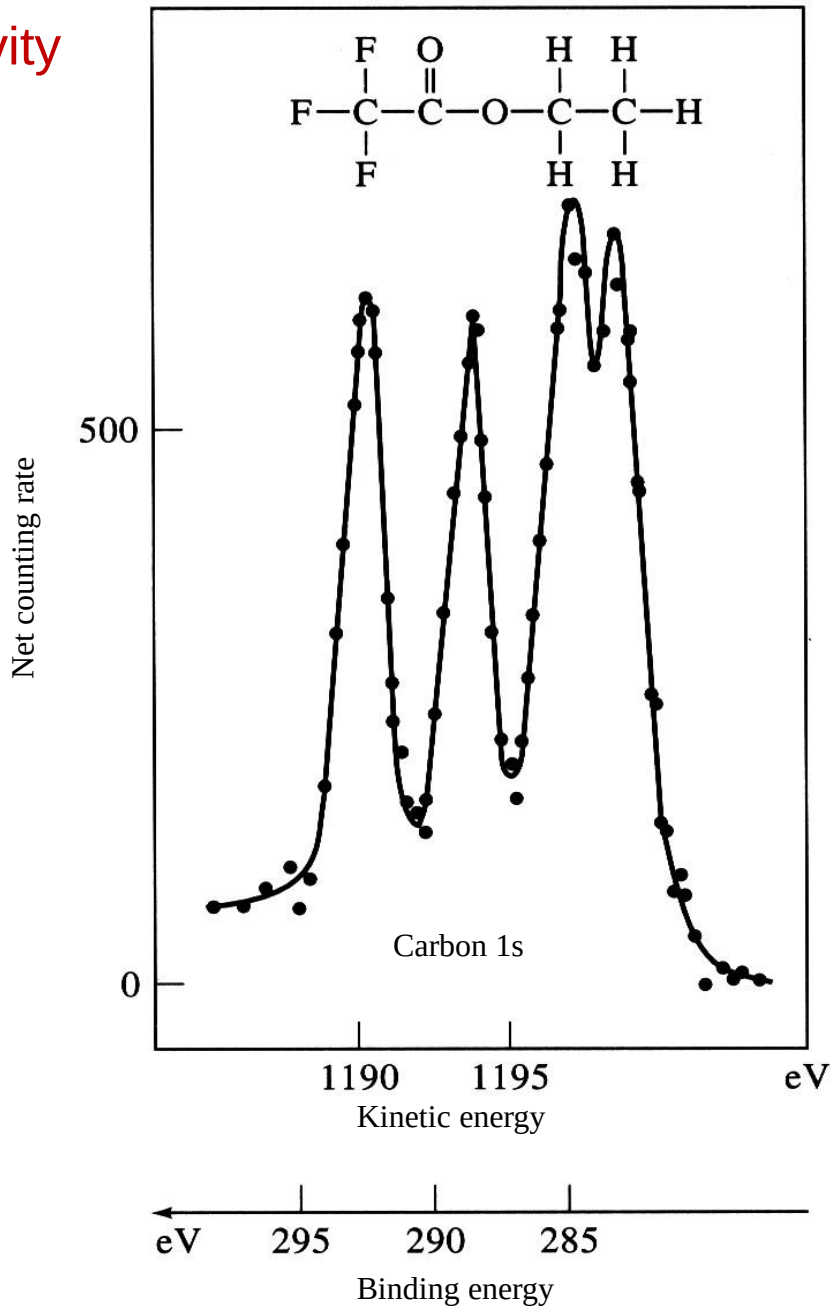

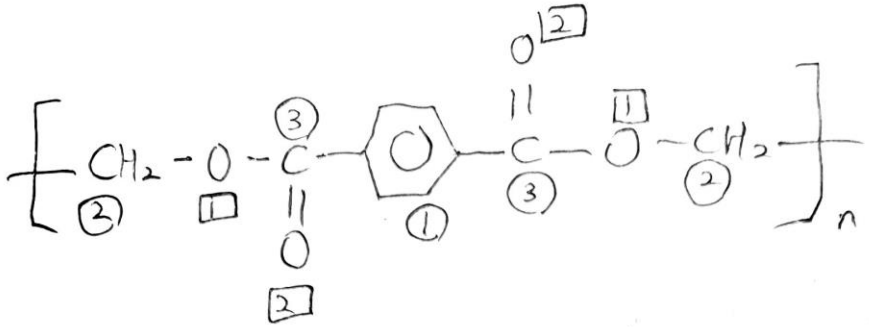

C(1s) screen effect ① > ② > ③

→ effective nuclear force ① < ② < ③

BE (binding energy) ① < ② < ③

intensity 6 : 2 : 2 = 3 : 1 : 1

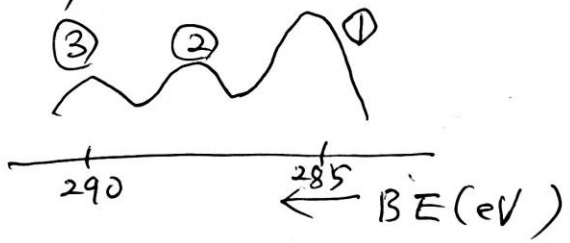

O(1s) screen effect [1] > [2]

BE [1] < [2], intensity 1 : 1

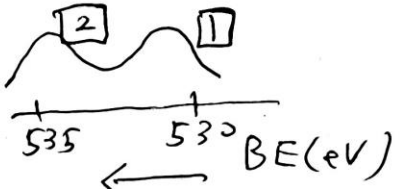

Inorganic structure → metal oxidation state

TABLE 21-2 Chemical Shifts as a Function of Oxidation State[a]

Element[b]	Oxidation State									
	−2	−1	0	+1	+2	+3	+4	+5	+6	+7
Nitrogen (1*s*)	—	*0[c]	—	+4.5[d]	—	+5.1	—	+8.0	—	—
Sulfur (1*s*)	−2.0	—	*0	—	—	—	+4.5	—	+5.8	—
Chlorine (2*p*)	—	*0	—	—	—	+3.8	—	+7.1	—	+9.5
Copper (1*s*)	—	—	*0	+0.7	+4.4	—	—	—	—	—
Iodine (4*s*)	—	*0	—	—	—	—	—	+5.3	—	+6.5
Europium (3*d*)	—	—	—	—	*0	+9.6	—	—	—	—

[a] All shifts are in electron volts measured relative to the oxidation states indicated by (*). (Reprinted with permission from D. M. Hercules, *Anal. Chem.*, **1970**, *42*, 28A. Copyright 1970 American Chemical Society.)

[b] Type of electrons given in parentheses.

[c] Arbitrary zero for measurement, end nitrogen in NaN_3.

[d] Middle nitrogen in NaN_3.

Oxidation state↑ → electron binding energy↑

Skoog, Holler, Crouch, Principles of Instrumental Analysis (Thomson)

XPS for Pt 4f levels:

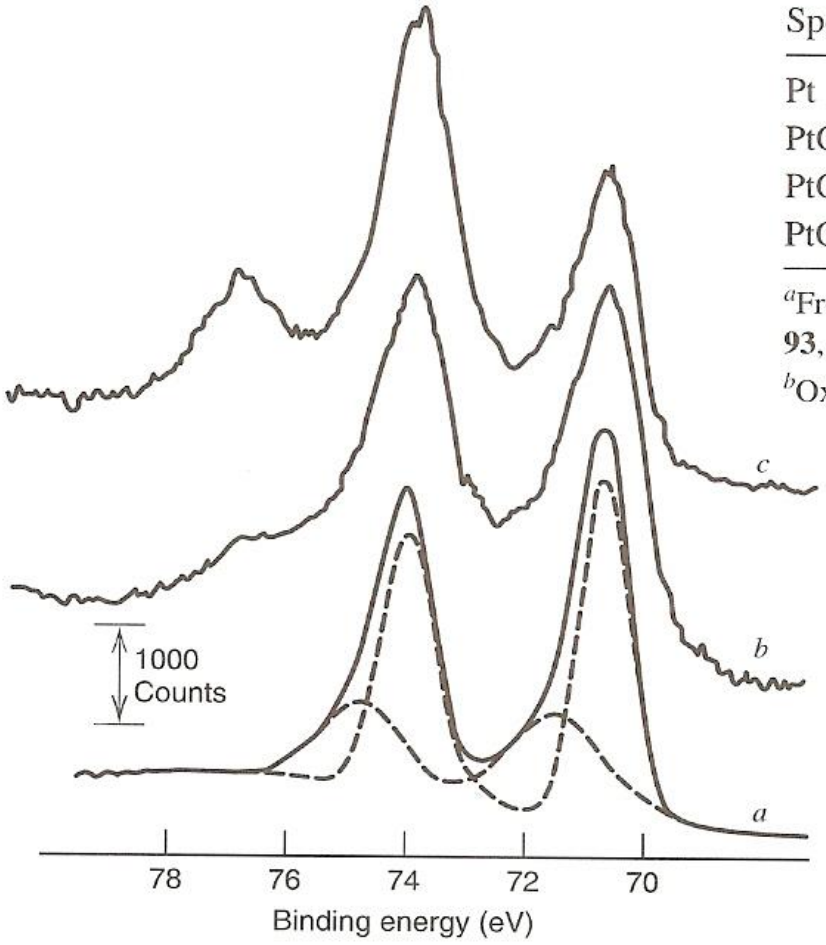

Species	Binding Energy, eV		Relative Peak Areas[b]		
	4f (7/2)	4f (5/2)	+0.7 V	+1.2 V	+2.2 V
Pt	70.7	74.0	56	39	34
PtO_{ads}	71.6	74.9	39	37	24
PtO	73.3	76.6	<5	24	22
PtO_2	74.1	77.4	0	0	20

[a]From K. S. Kim, N. Winograd, and R. E. Davis, *J. Am. Chem. Soc.*, **93**, 6296 (1971).

[b]Oxidation carried out at indicated potential (*vs.* SCE) for 3 min.

Shake-up satellite

"shake-up" peak at a higher binding energy than the main line. Shake up lines are common with paramagnetic states.

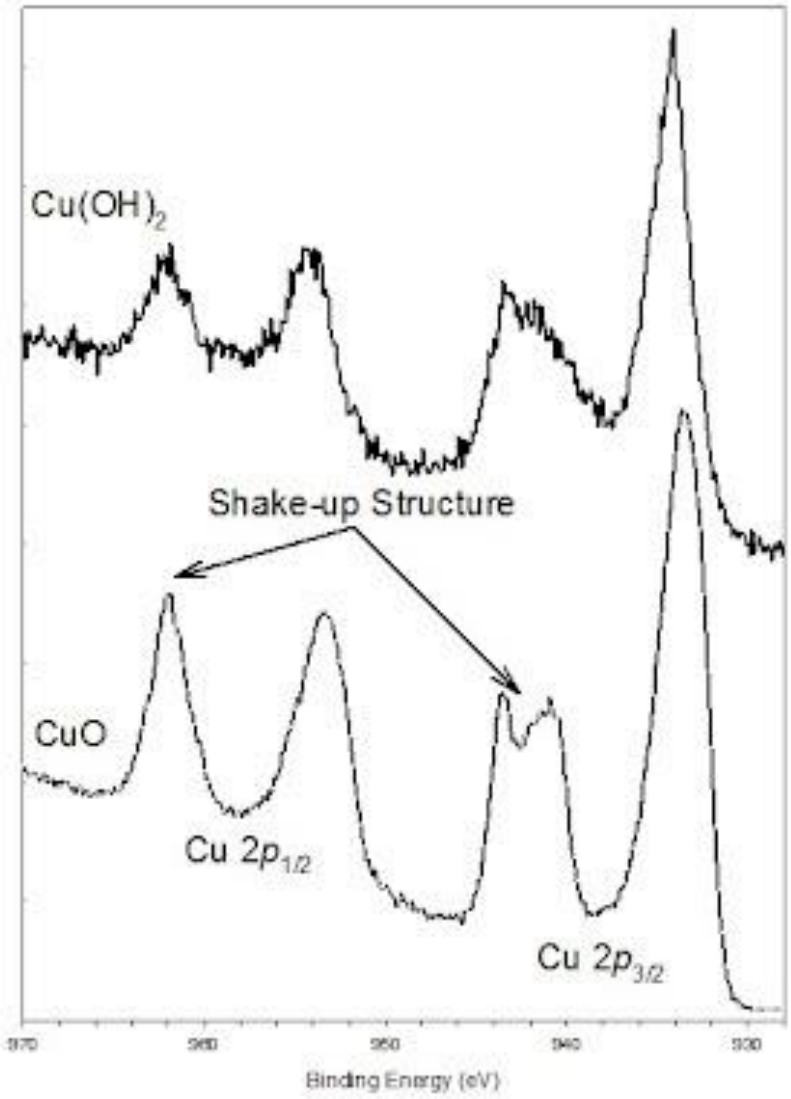

cf. Shake-off satellite

+ excitation valence electron to continuum

M.C. Biesinger, L.W.M. Lau, A.R. Gerson, R.St.C. Smart, *Appl. Surf. Sci.* **257** (2010) 887.

XPS data analysis

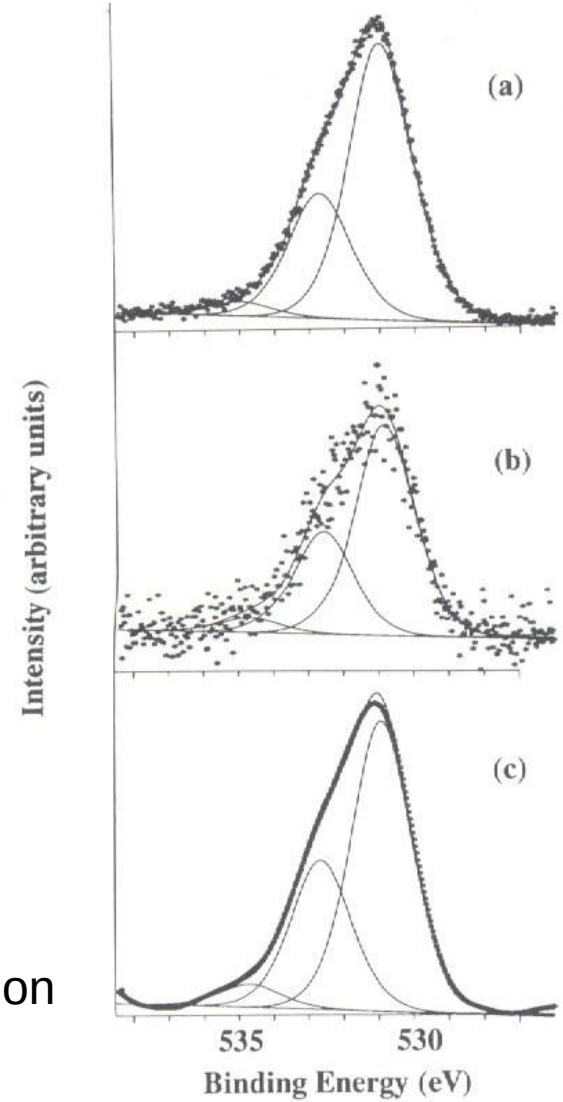

deconvolution

Figure A3.2 Oxygen 1*s* spectra illustrating the effect of smoothing. In all cases the spectra are fitted to three peaks. (a) Data for the same material obtained with good statistics by running the spectrum for a long period (82 scans), (b) data for the same material with bad statistics by running the spectrum for a short period (2 scans) and (c) the result of smoothing (b) 100 times with a smoothing interval of 21

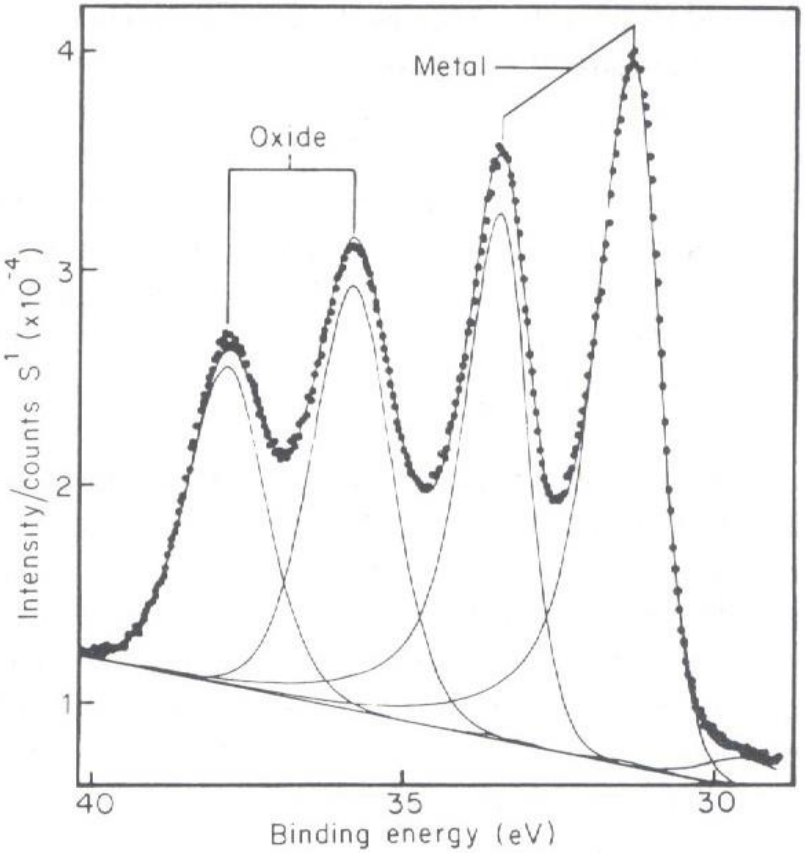

Figure A3.6 Curve-fitted W 4*f* spectrum

D. Briggs, M. P. Seah, *Practical Surface Analysis*, Wiley

XPS quantitative analysis

$$I = n\phi\sigma\varepsilon\eta ATl \qquad (21\text{-}3)$$

Sensitivity factor

$$S = \sigma\varepsilon\eta ATl \qquad (21\text{-}4)$$

n: number density of atoms of the sample (atoms/cm^3)
φ: flux of the incident X-ray beam (photons/cm^2·s)
σ: photoelectric cross section (cm^2/atom)
ε: angular efficiency factor for the instrument
η: the efficiency of producing photoelectrons (photoelectrons/photon)
A: area of sample which photoelectrons are detected (cm^2)
T: the efficiency detection of the photoelectrons
l: mean free path of photoelectrons in the sample (cm)

→ for a given transition, last six terms are constant → atomic sensitivity factor s (in XPS Handbook)

$I/s \propto$ concentration

Electrochemical XPS (SNU)

UHV-XPS

Glove Box

Ex-situ Analysis without Contamination

Ambient Pressure X-ray Photoelectron Spectroscopy

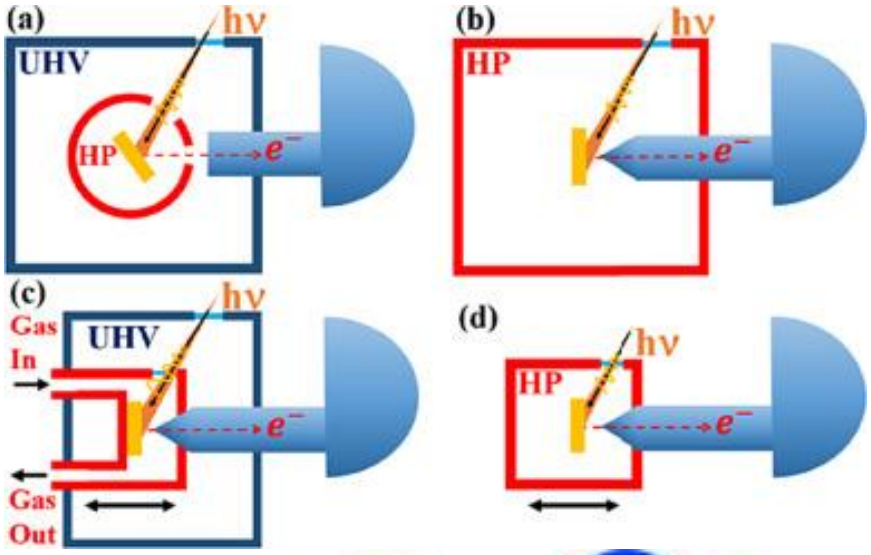

John T. Newberg et al, Surface Science Reports, 73, 37 (2018).

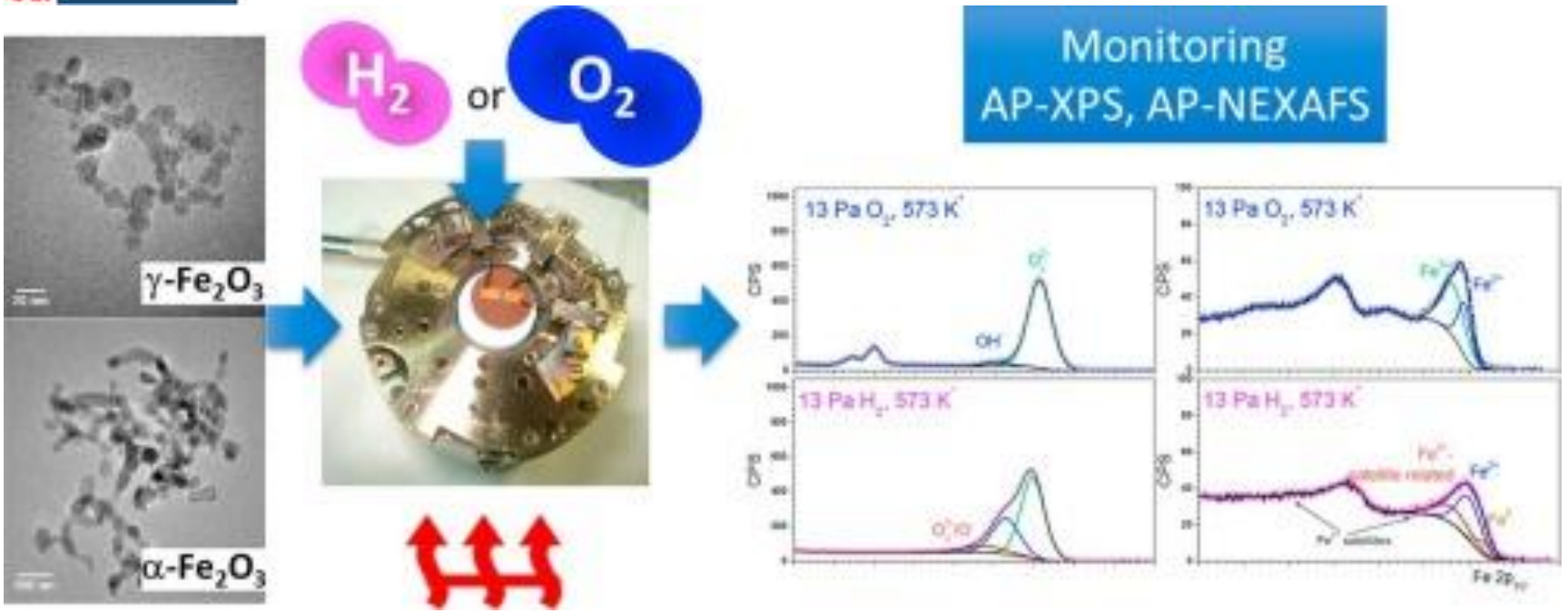

Dorota Flak *et al*, Applied Surface Science, 455, 1019-1028 (2018).

Ultraviolet photoelectron spectroscopy (UPS)

UV source: atomic lamps, He (21.1, 42.82 eV)

UV photons can excite photoemission from valence levels
Since valence electrons are involved in chemical bonding → UPS is well suited to the study of bonding at surfaces → work function, band structure of the solids, surface and adsorbed layers, bonding structure(σ or π)

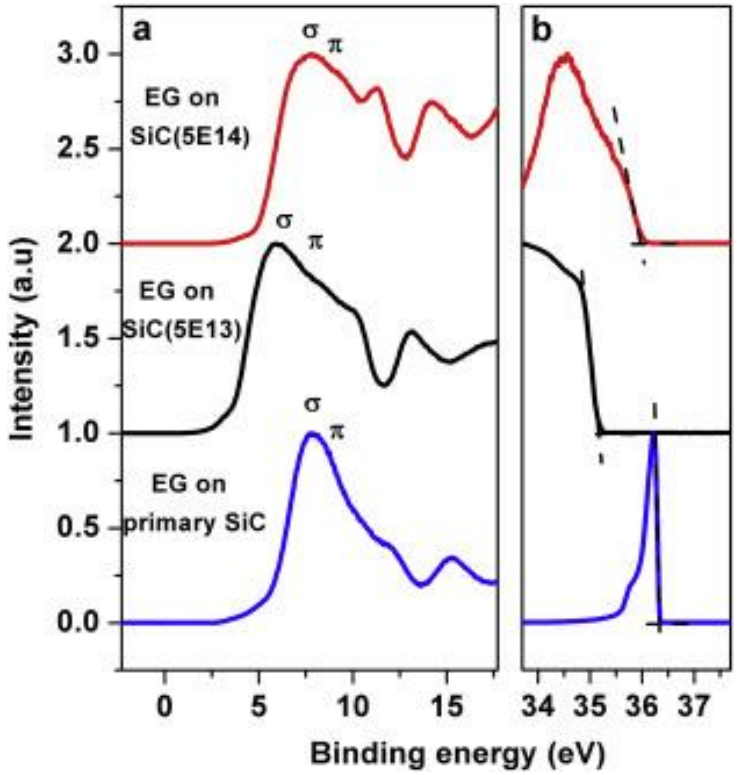

Hui Guo *et al*, Carbon, 157, 340 (2020).

Auger electron spectroscopy (AES)

3 electron processes

(1) Core electron ejected

(2) Higher electron fills the core hole

(3) Exothermicity to eject 3rd electron (Auger electron)

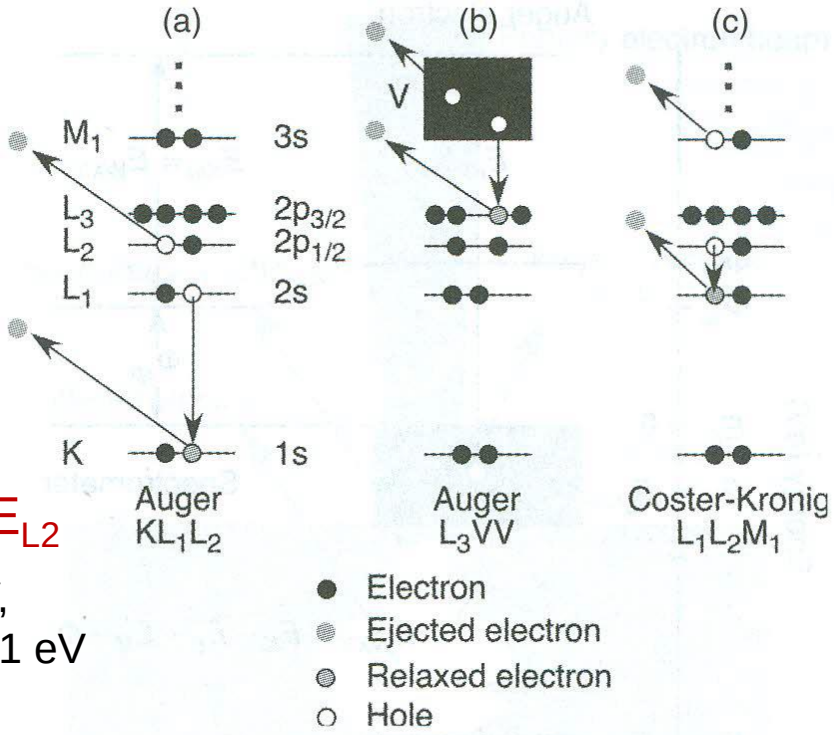

$E_{KL1L2} = (E_K - E_{L1}) - E_{L2}$

E_K = 532 eV, E_{L1} = 24 eV,
E_{L2} = 7 eV → E_{KL1L2} = 501 eV

Figure 2.22 *A detailed depiction of Auger transitions involving (a) three core levels; (b) two core levels and the valence band; and (c) a Coster-Kronig transition in which the initial hole is filled from the same shell.*

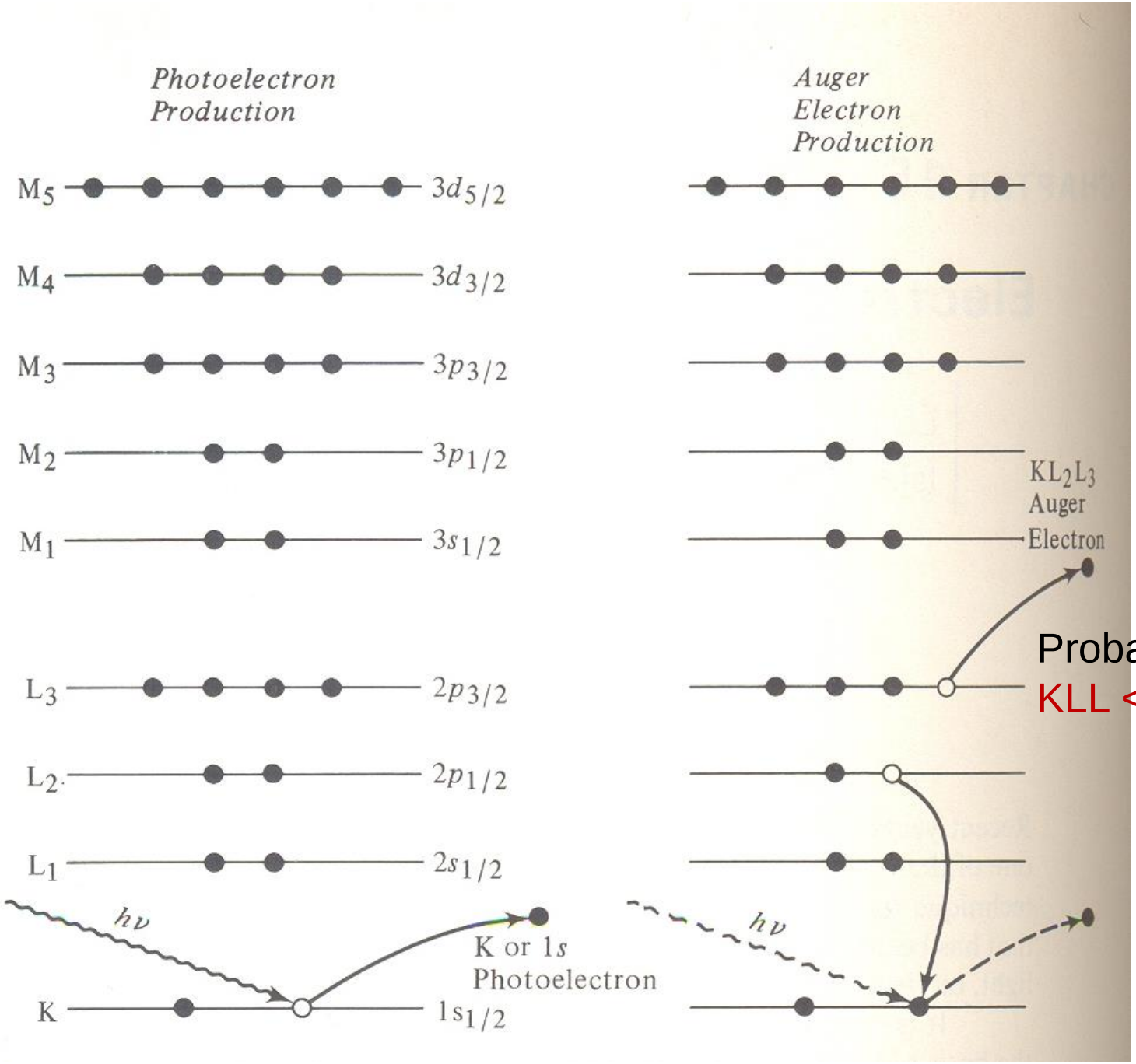

Probability

KLL < LMM < MNN

AES Signal (small peak, hard to define exact peak) → dN(E)/dE

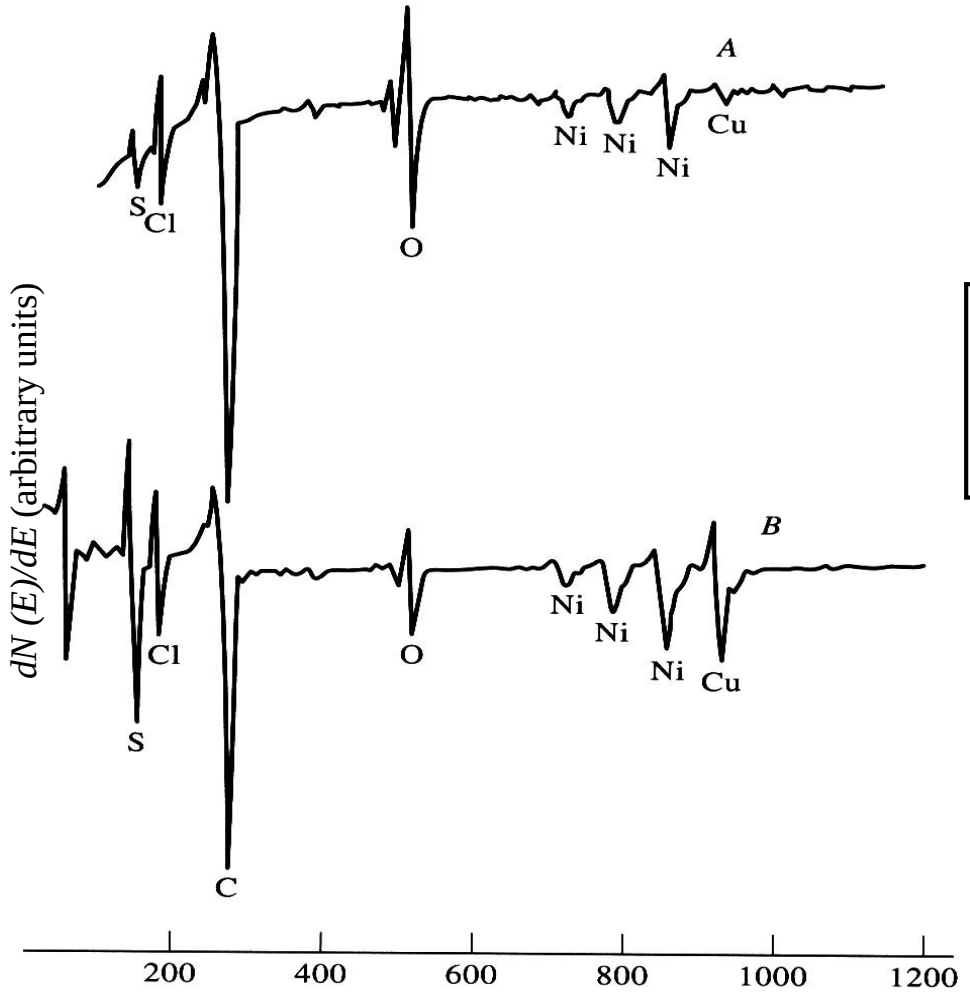

Auger Electrons

→ element analysis

✓ Oxidation state

✓ Structure

AES quantitative analysis

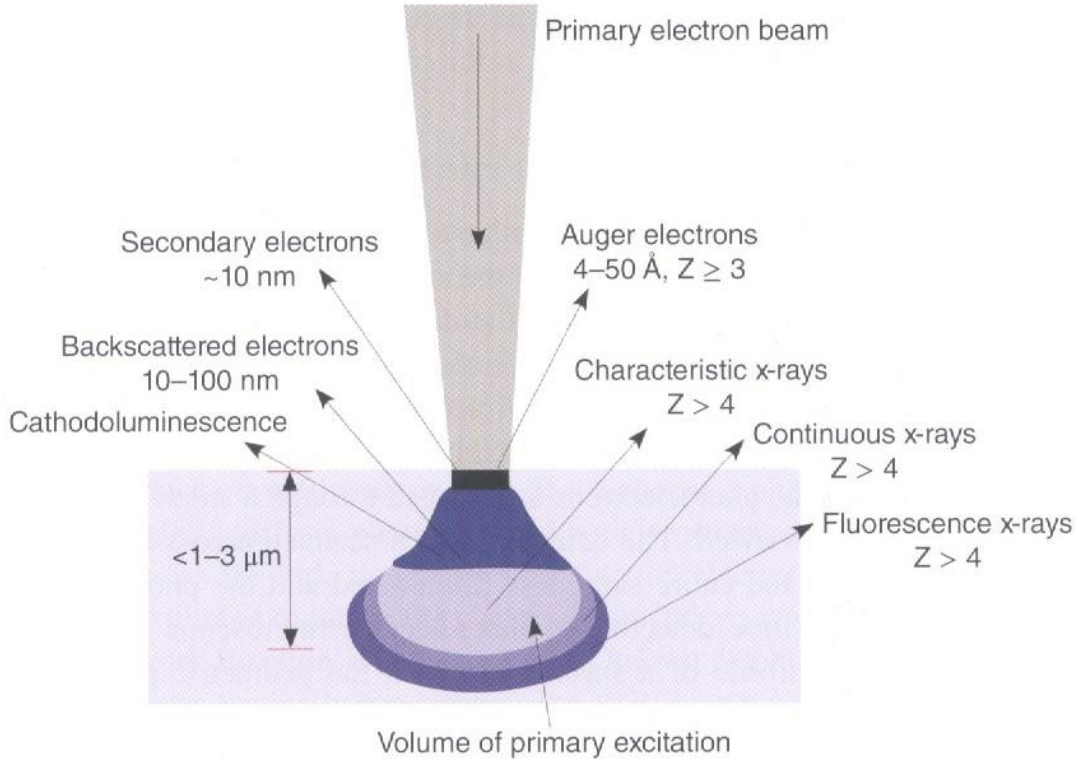

Figure 2.24 *The geometry of Auger electron spectroscopy. A primary electron beam excites the formation of Auger electrons as well as X-ray fluorescence. Backscattered and secondary electrons are also created in the process.*

Approximate compositional analysis can easily be obtained with the use of the measured relative sensitivity factors s_X, which can be found in the *Handbook of Auger Electron Spectroscopy* [116]. The mole fraction of component A in a binary mixture of A and B is given by

$$x_A = \frac{I_A/s_A}{I_A/s_A + I_B/s_B}. \qquad (2.6.30)$$

AES depth profile: ion sputtering

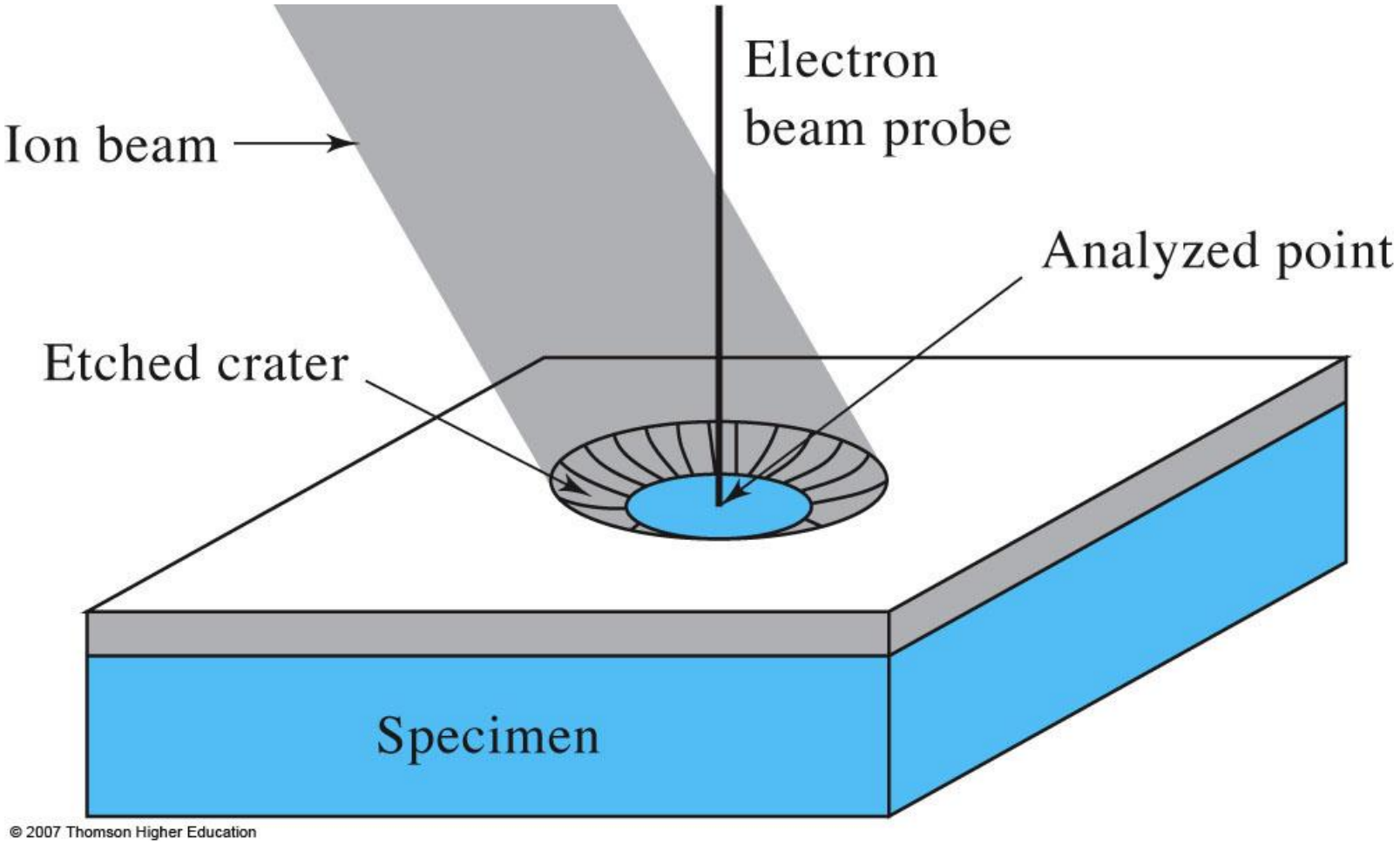

Skoog, Holler, Crouch, Principles of Instrumental Analysis (Thomson)

AES depth profiles: GaAs

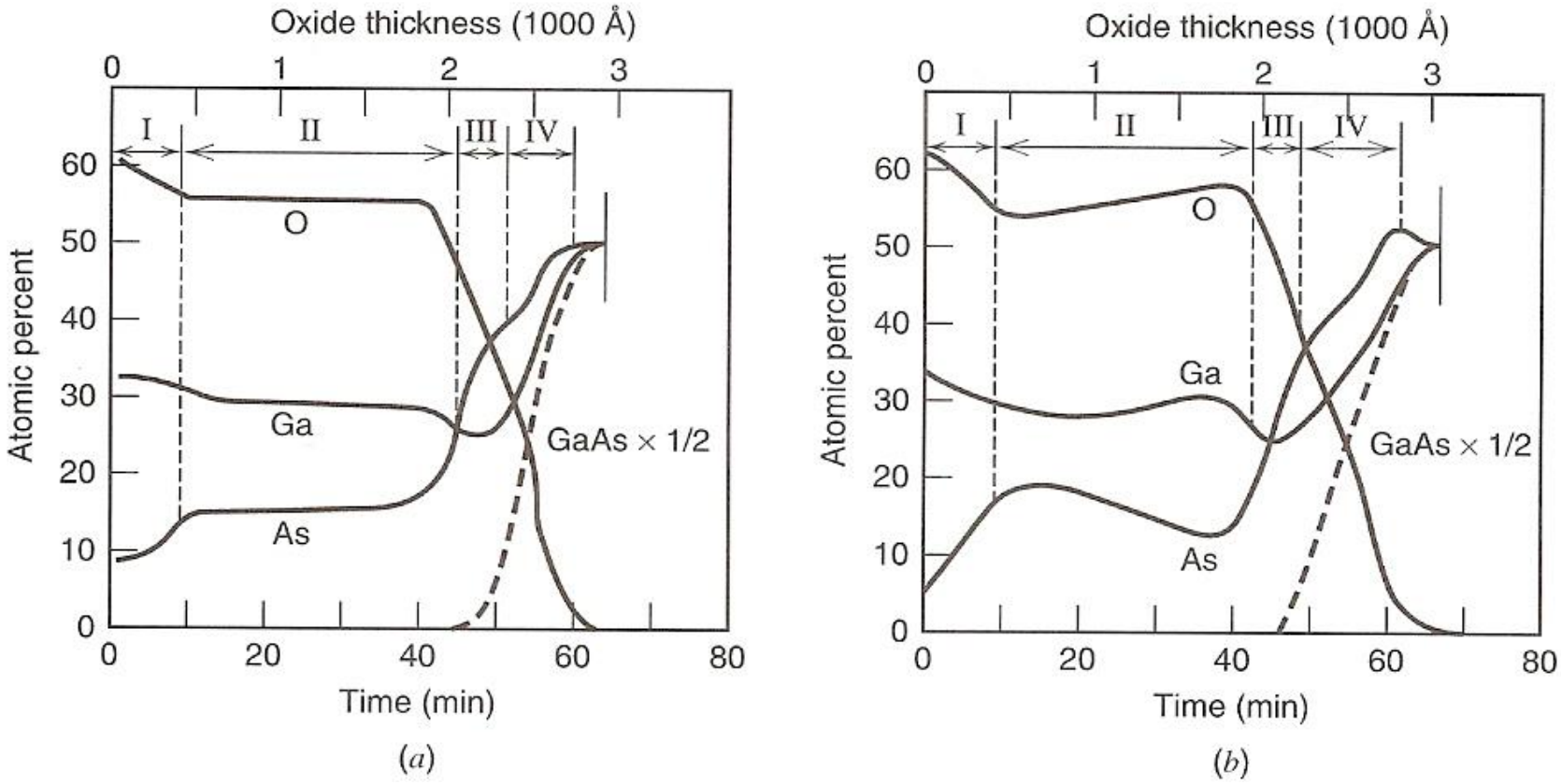

Vibration spectroscopy

Vibration motions → IR absorption, electron energy loss, Raman, sum frequency generation, inelastic neutron tunneling, He scattering

Energy of electromagnetic field: oscillating electric & magnetic disturbance

$$E = h\nu = h\,c/\lambda$$

h; Planck constant (6.6×10^{-34} Js)
speed of light (c); 3×10^{8} m/s,
wavelength (λ); distance between the neighboring peaks of wave,

$$1\ \text{Å} = 0.1\ \text{nm} = 10^{-10}\ \text{m}$$

frequency (ν, Hz = 1 s^{-1}); number of times per second

$$\lambda\nu = c$$

wavenumber (cm^{-1}, reciprocal cm), $\bar{\nu}$ = $\nu/c = 1/\lambda$
cf) 1 eV ~ 8066 cm^{-1}

Wavelength (λ, nm) = 1240/band gap energy (eV)

Electron energy loss spectroscopy (EELS)

Electron backscattered from surface → lose energy of the surface and adsorbed layer → vibrational transitions (1 meV = 8.064 cm^{-1})

$$E = E_0 - \hbar\omega$$

cf.

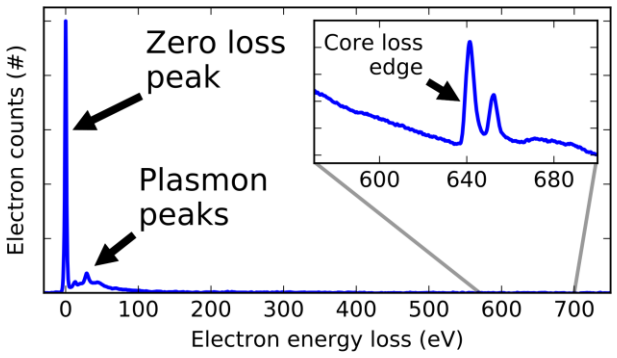

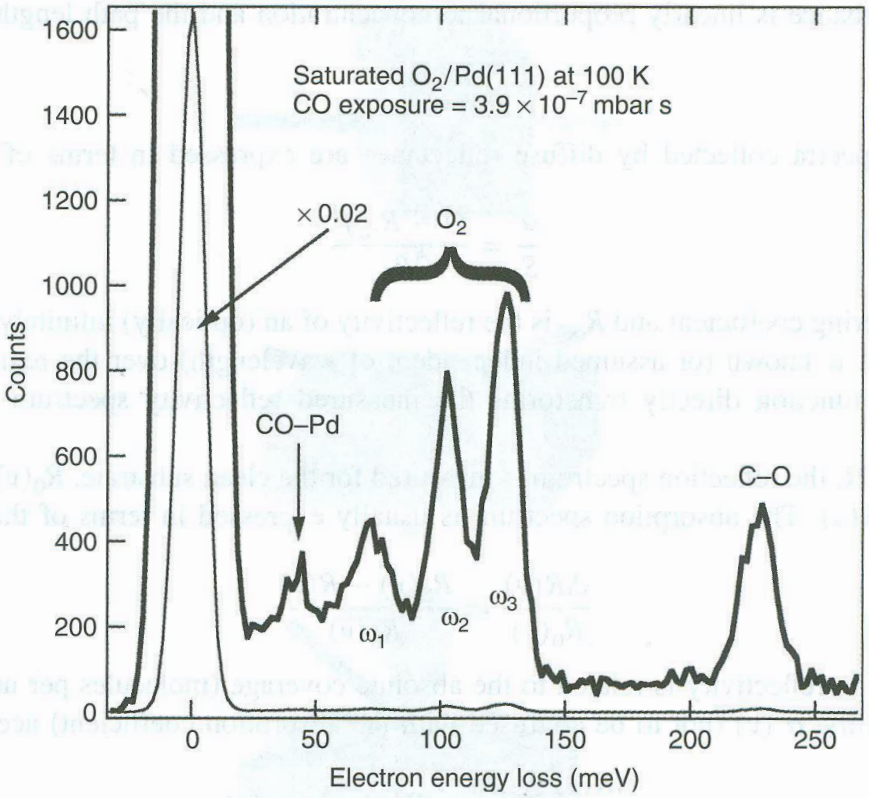

Figure 2.29 *The electron energy loss spectrum of co-adsorbed O_2 + CO on Pd(111). The species associated with ω_1, ω_2 and ω_3 are illustrated in Fig. 3.8. Adapted from K.W. Kolasinski, F. Cemič, A. de Meijere, E. Hasselbrink, Surf. Sci., 334, 19. © 1995 with permission from Elsevier.*

High resolution electron energy loss spectroscopy (HREELS)

a tool used in surface science.
The inelastic scattering of electrons from surfaces is utilized to study electronic excitations or vibrational modes of the surface of a material or of molecules adsorbed to a surface. In contrast to other electron energy loss spectroscopies (EELS), HREELS deals with small energy losses in the range of 10^{-3} eV to 1 eV. It plays an important role in the investigation of surface structure, catalysis, dispersion of surface phonons and the monitoring of epitaxial growth. (Wikipedia)

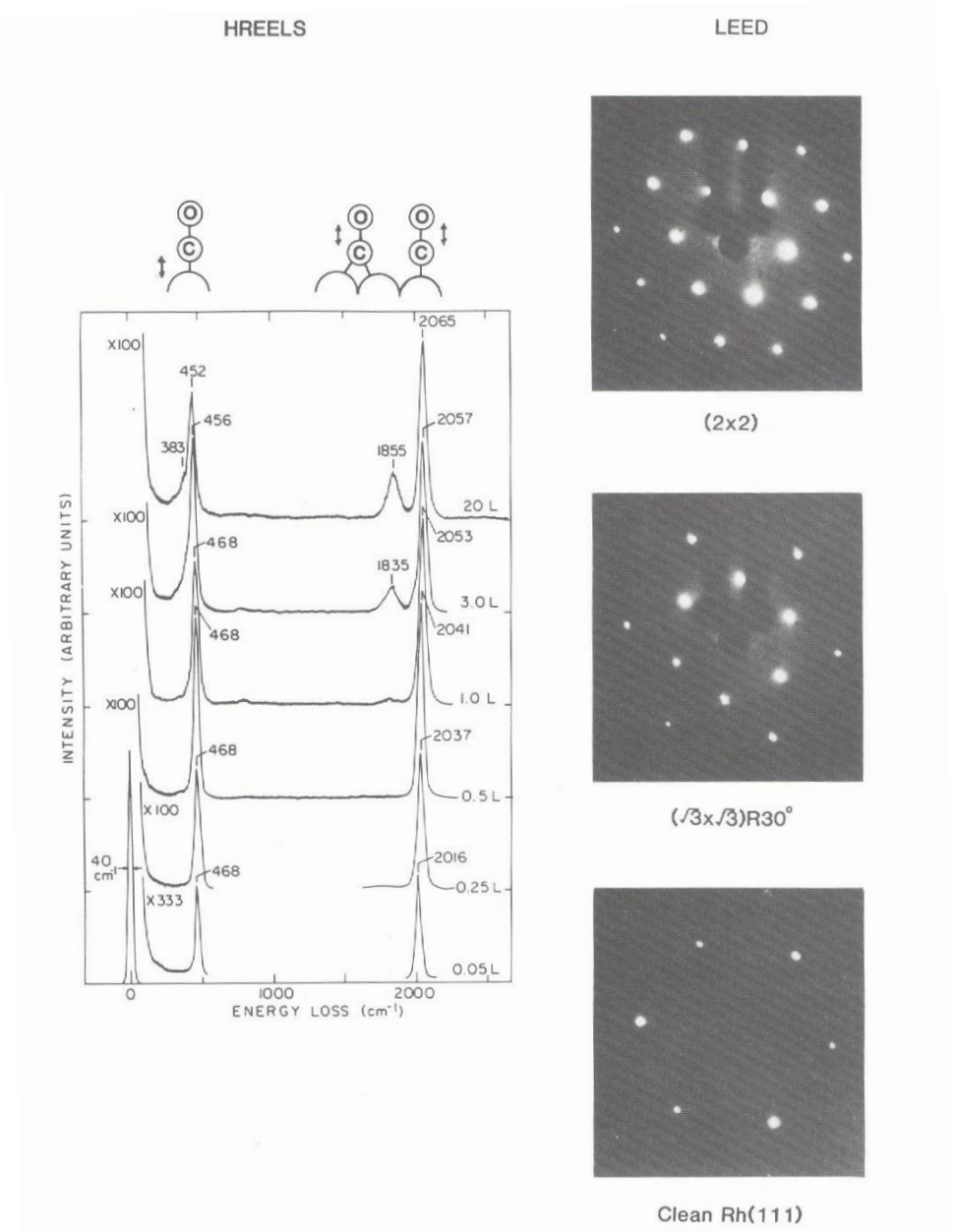

Figure 4.4. Vibrational spectrum of carbon monoxide chemisorbed on the Rh(111) surface obtained by HREELS. The curves correspond to the spectrum obtained at different CO exposures, *L*. The LEED diffraction pattern indicates that the CO monolayer is ordered at the different coverages.

Somorjai,
Introduction to Surface Chemistry and Catalysis

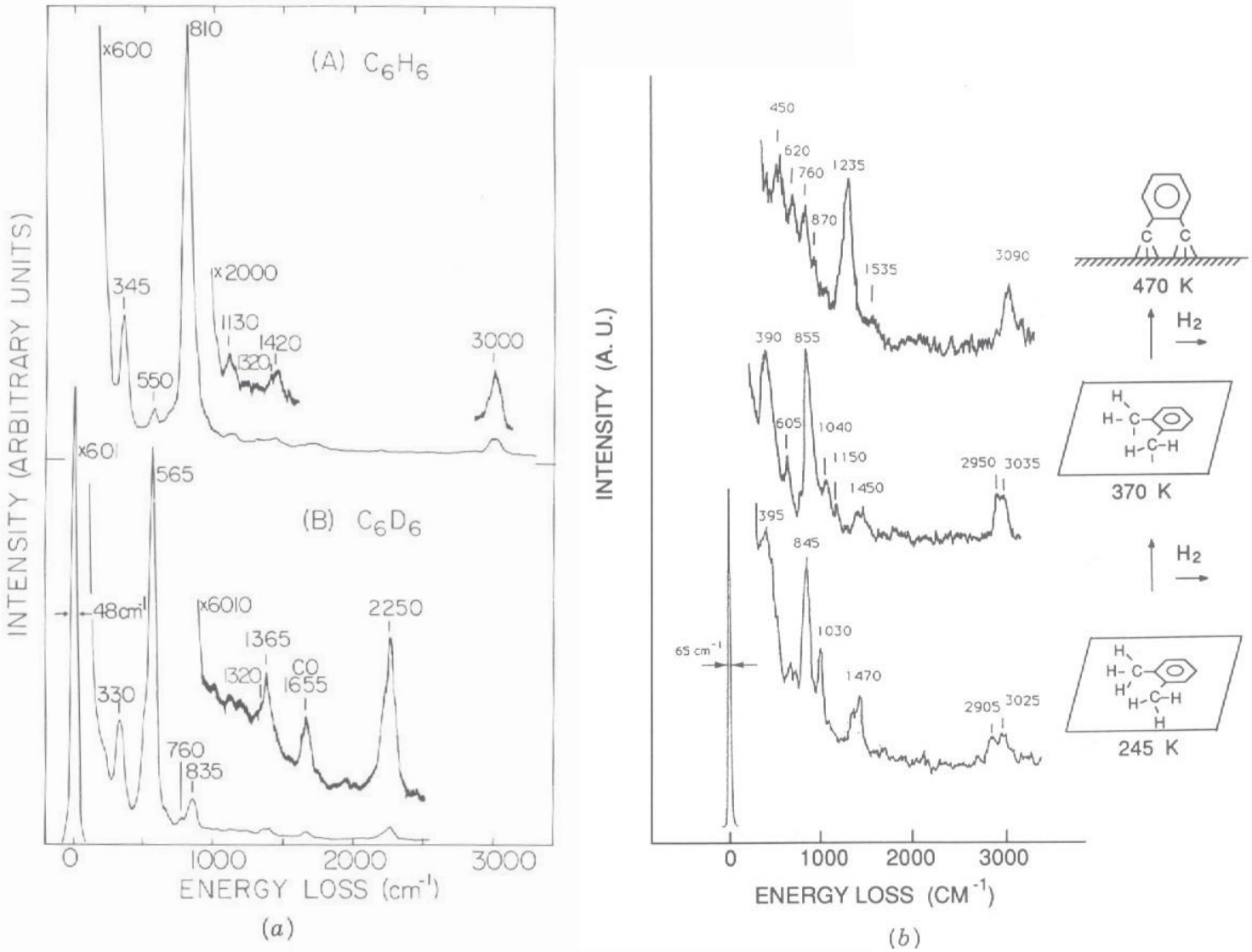

Figure 4.5. **(a)** Vibrational spectra obtained by HREELS in the specular direction for a saturation coverage of benzene chemisorbed on Rh(111) at 300 K for a well-ordered $c(\sqrt{3} \times 4)$ surface structure: **(A)** C_6H_6; **(B)** C_6D_6 [90]. **(b)** The vibrational spectra of *o*-xylene at three different temperatures [91].

Somorjai, *Introduction to Surface Chemistry and Catalysis*

Summary

- Knudsen beams are molecular beams with thermal properties.
- Supersonic jets experience significant cooling during expansion, exhibit high-translational energy and have significantly enhanced intensity compared to Knudsen beams.
- STM involves the tunnelling of electrons from occupied to unoccupied electronic states. The voltage between the tip and the surface determines the direction of current flow.
- STM images electronic states not atoms.
- AFM allows for atomic scale imaging on insulating surfaces and for direct measurements of intermolecular forces.
- NSOM extends optical spectroscopy to the nanoscale and even single molecule regime.
- Low-energy (~20–500 eV) electrons penetrate only the first few atomic layers and can be used to investigate surface structure.
- The symmetry of LEED patterns is related to the periodicity of the substrate and adsorbate overlayer structure.
- XPS probes the electronic states associated with core levels and is particularly well suited to quantitative elemental analysis.
- UPS probes the electronic states associated with valence electrons, and is particularly well suited to the study of electronic changes associated with chemical bonding.
- AES is also used for quantitative elemental analysis.
- In IR spectroscopy at metal surfaces, a strict dipole selection rule means that only vibrations with a component along the surface normal can be observed.
- In EELS electrons scatter through dipole, impact and/or resonance scattering mechanisms, and no strict selection rule can be assumed unless the mechanism is known.
- EELS is suitable for the investigation of low-frequency vibrational modes.
- SHG and SFG can be interface sensitive even in the presence of a gas or liquid.
- SFG can be used not only to perform spectroscopy in the frequency domain, but also to perform pump-probe studies, which investigate dynamics directly in the time domain.

Additional Note

(This content is not the scope of the exam.)

Scanning probe techniques

→ Surface structure, manipulation of atoms & molecules at surface

-Microscopy: a sharp tip close to the surface → scanning electron or force and so on → STM, AFM and so on
-Similar idea: NSOM (Near field scanning optical microscopy) → a small-diameter optical fiber close to the surface (diameter/distance < wavelength of the light) → image resolution far below light wavelength
-SP techniques: current, van der Waals force, chemical force, magnetic force, capacitance, phonon, photon
-UHV or at atmosphere or in solution, *in situ vs. ex situ* techniques

Scanning tunneling microscopy (STM)

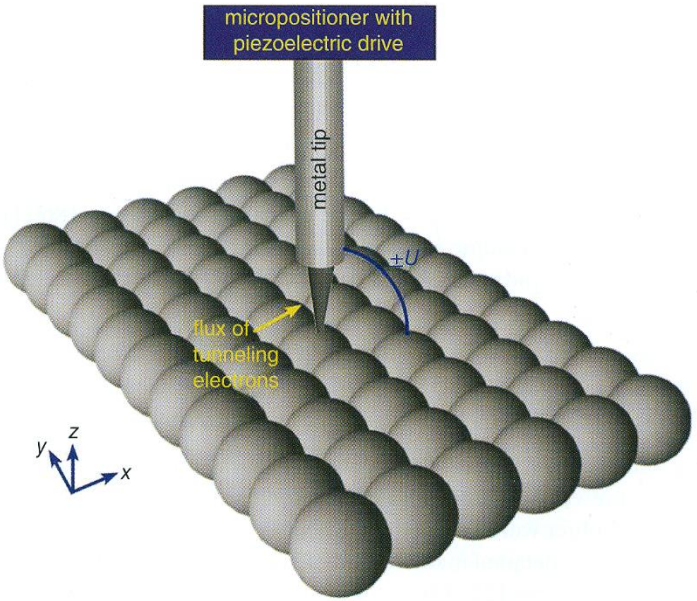

Tersoff and Hamann [31, 32] set the theoretical basis for interpretation of STM images. The tunnelling current, I, depends exponentially on the tip to surface distance d according to

$$I \propto e^{-2\kappa d} \tag{2.4.3}$$

where the decay constant κ is given by

$$\kappa = \frac{1}{\hbar}\sqrt{2m_e(\Phi_s + E_F^s - E)}. \tag{2.4.4}$$

E is the energy of the state from which tunnelling occurs, and the barrier height is given by the sum of the average work function of the sample surface Φ_s and its Fermi energy E_F^s. κ is on the order of 1 $Å^{-1}$, hence, a change in separation of just 1 Å leads to an order of magnitude change in the tunnelling current. Importantly, STM does not rely on simple one-dimensional tunnelling but is instead sensitive

cf. Tunnelling

- if the potential energy of a particle does not rise to infinite in the wall & $E < V \rightarrow \Psi$ does not decay abruptly to zero
- if the walls are thin $\rightarrow \Psi$ oscillate inside the box & on the other side of the wall outside the box $\rightarrow$ particle is found on the outside of a container: leakage by penetration through classically forbidden zones “tunnelling”

cf) C.M.: insufficient energy to escape

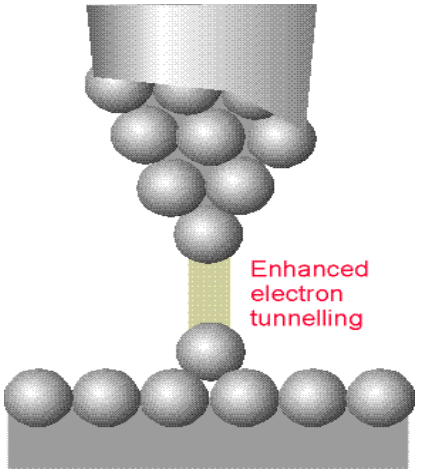

Electron flow between tip and surface

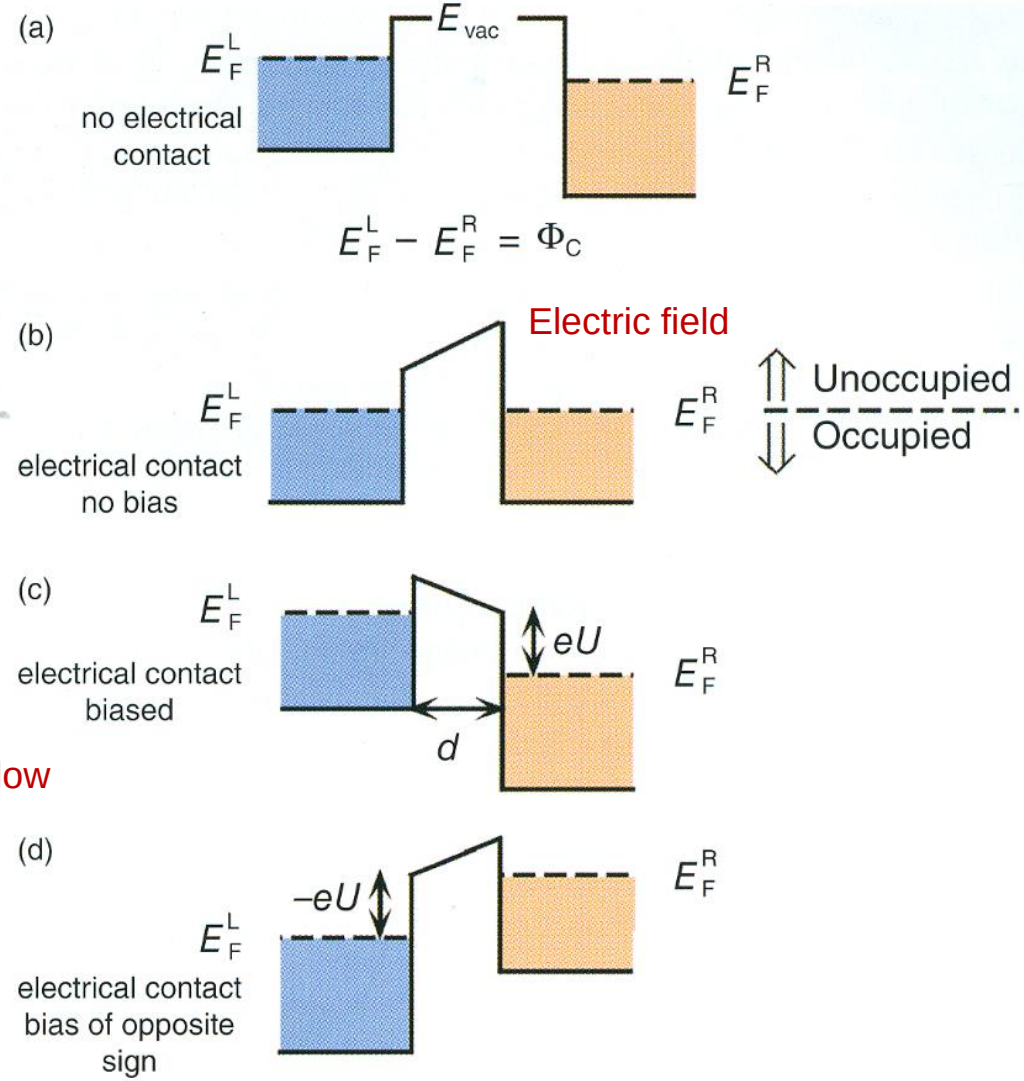

Tunneling current flow

Figure 2.7 *Illustrations of the Fermi and vacuum level positions for two metals separated by distance* d. *(a) Isolated metals. (b) After electrical contact, in the absence of an applied bias. (c) Biasing shifts the relative positions of the Fermi levels and makes available unoccupied states in an energy window* eU *into which electrons can tunnel. (d) The direction of tunnelling is switched compared to the previous case simply by changing the sign of the applied bias.*

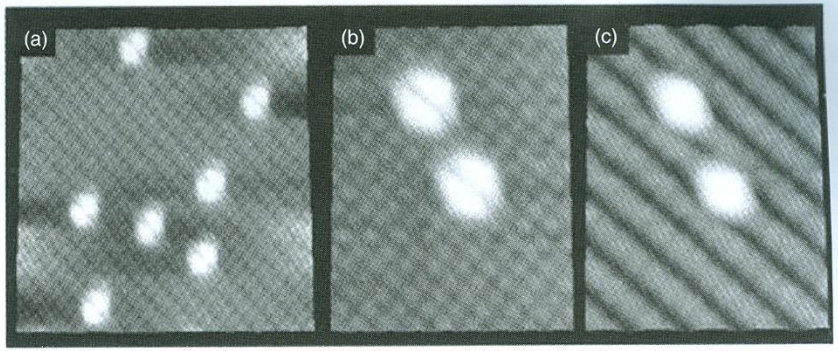

Figure 2.4 *An STM image of occupied states on a Si(100)-(2 × 1) surface nearly completely covered with adsorbed H atoms. The uncapped Si dangling bonds (sites where H is not adsorbed) appear as lobes above the plane of the H-terminated sites. The rows of the (2 × 1) reconstruction are clearly visible in the H-terminated regions. Source: Reproduced from J.J. Boland,* Phys. Rev. Lett. ***67*** *(1991) 1539. (c) 1991, with permission from the American Physical Society.*

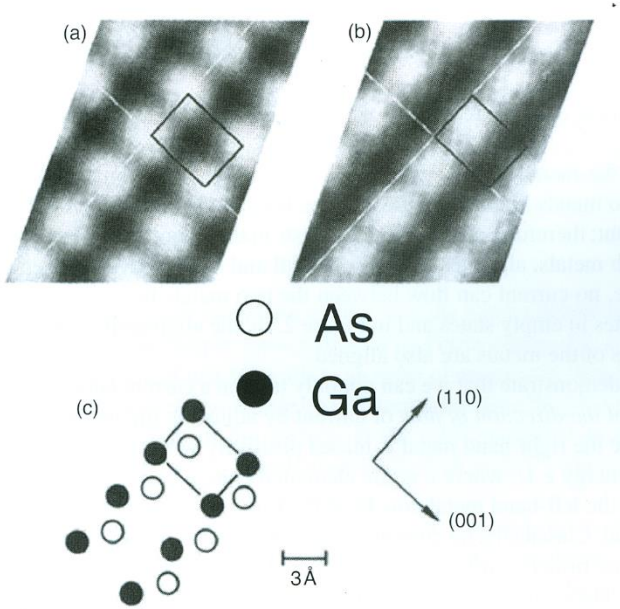

Figure 2.5 *Constant current STM images of the clean GaAs(110) surface. (a) The normally unoccupied states imaged at* V = +1.9 V. *(b) The normally occupied states imaged at* V = −1.9 V. *(c) Schematic representation of the positions of the Ga (•) and As (o) atoms. The rectangle is at the same position in (a), (b) and (c). This is an unusual example of chemically specific imaging based simply on the polarity of the tip. Source: Reproduced from R.M. Feenstra, J.A. Stroscio, J. Tersoff and A.P. Fein,* Phys. Rev. Lett. ***58*** *(1987) 1192. (c) 1987, with permission from the American Physical Society.*

Electrochemical STM

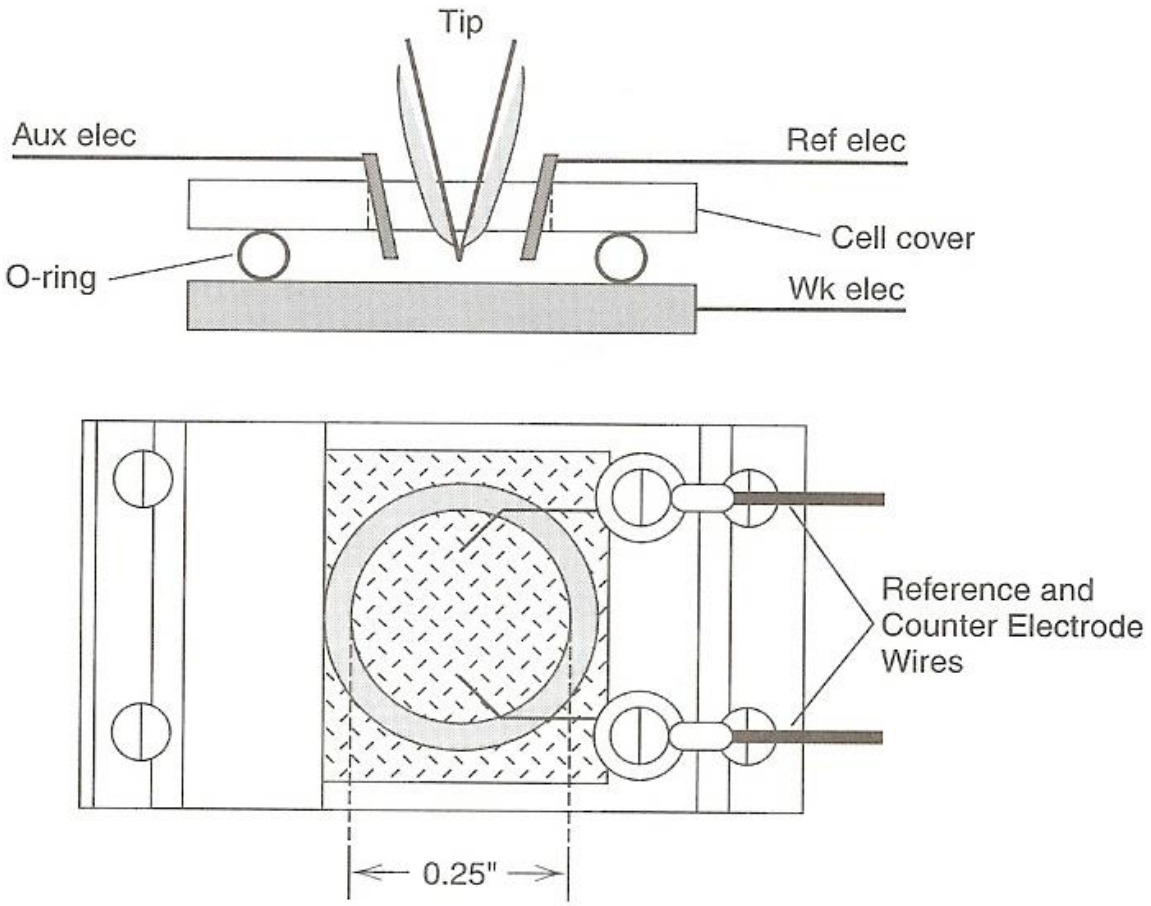

Scanning tunneling spectroscopy (STS)

STM image depends on the voltage on the tip → control of the voltage → to determine the electronic states with atomic resolution (STS)

Chemisorption changes the electronic structure of the surface

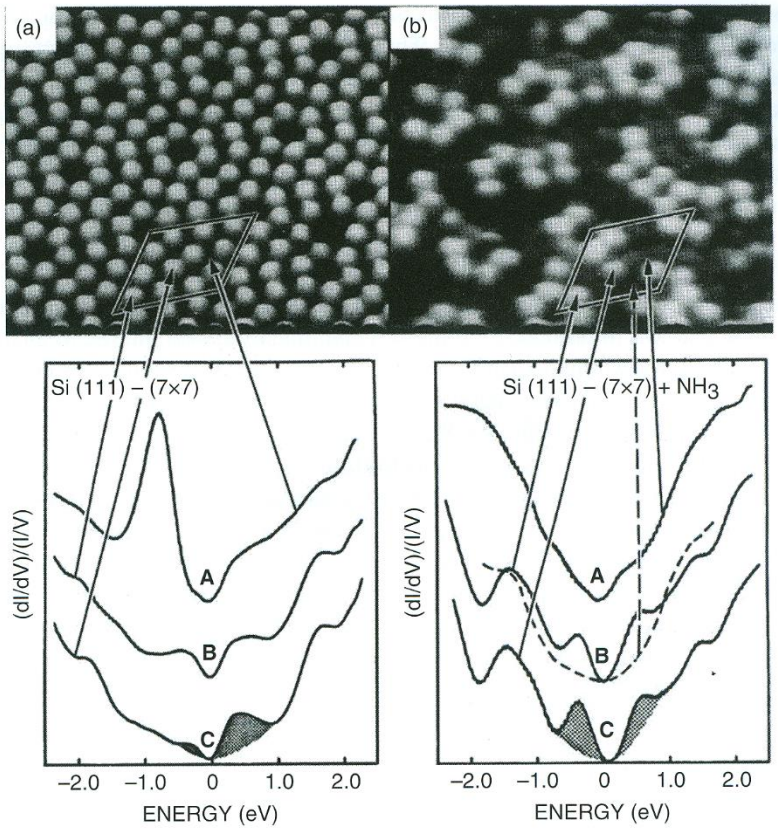

Figure 2.8 *Left-hand side: Topography of the unoccupied states of the clean (7×7) surface (top panels) and atom resolved tunnelling spectra (bottom panels). The curves represent spectra acquired over different sites in the reconstructed surface (Curve A: restatom, Curve B: corner adatom, Curve C: middle adatom). Negative energies correspond to occupied states, positive to empty states. Right-hand side: Same types of images and spectra obtained after exposure of a Si(111)-(7×7) surface to NH_3. The different sites exhibit different reactivities with respect to NH_3 adsorption with the restatoms being the most reactive and the middle adatoms being the least reactive. Source: Reproduced with permission from Ph. Avouris and R. Wolkow, Phys. Rev. B 39 (1989) 5091. © 1989 American Physical Society.*

Scanning electrochemical microscopy (SECM)

Using ultra-micro electrode or nano-electrode

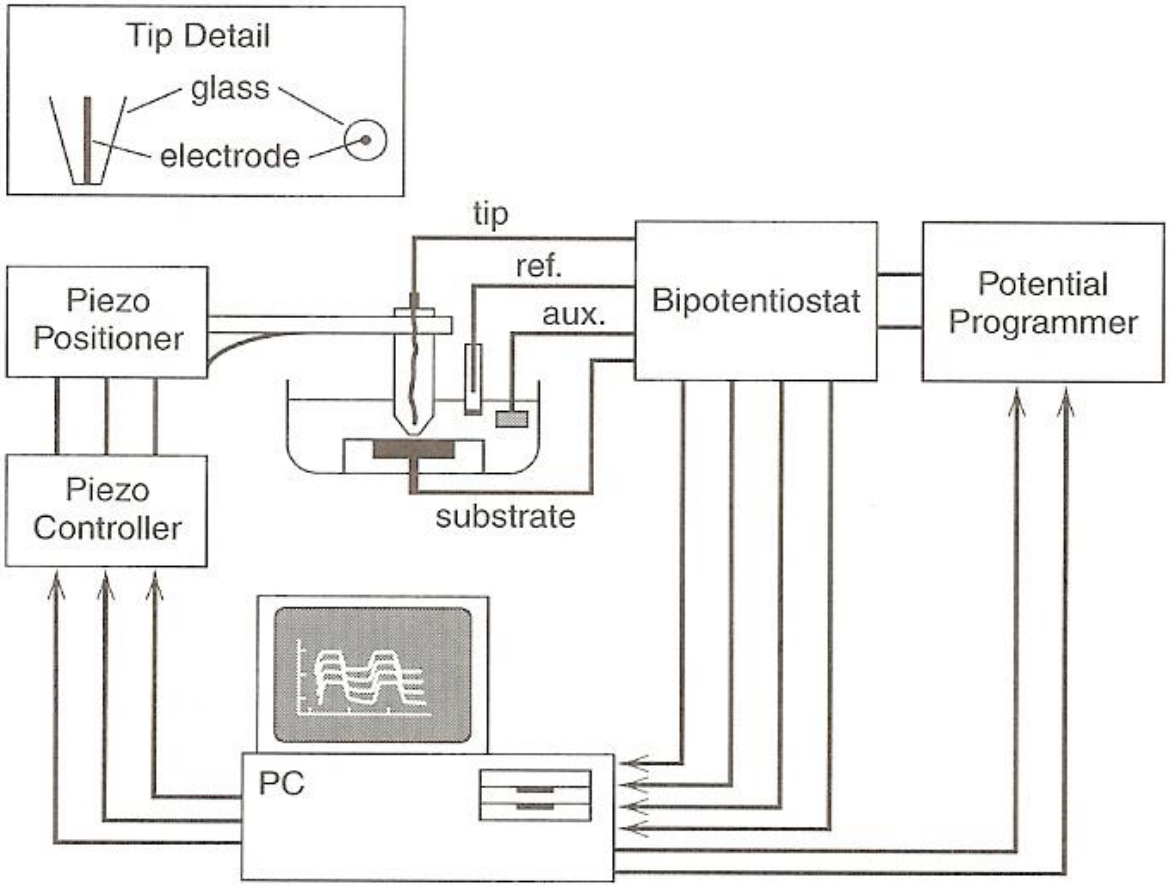

Atomic force microscopy (AFM)

-using attractive or repulsive interactions with the surface (Table 2.2): van der Waals….
-AFM can image conducting as well as insulating surfaces (soft, polymer, biological)
-Force curve: function of distance of the tip from the surface

Force

$$F_N = k_N \cdot \Delta z$$

k_N: force constant
Δz: displacement of the tip

Table 2.2 *Interaction forces appropriate to scanning force microscopy and their ranges.*

Force	Range (nm)
Electrostatic	100
Double layer in electrolyte	100
van der Waals	10
Surface-induced solvent ordering	5
Hydrogen bonding	0.2
Contact	0.1

Values taken from Takano et al. [45].

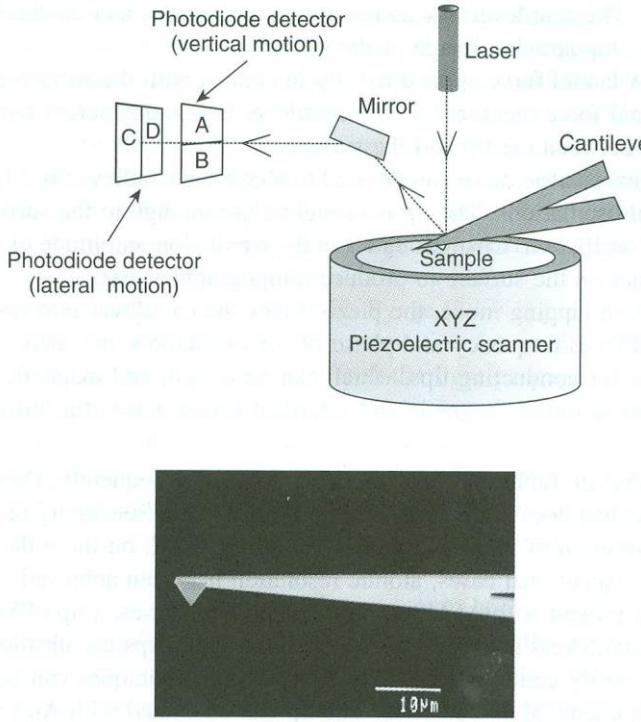

Figure 2.9 *Principal components for an optical lever type AFM. Detection of the reflected laser beam with a quadrant, position sensitive photodiode facilitates the simultaneous detection of bending and torsion of the cantilever. A scanning electron micrograph of a typical AFM cantilever and tip is shown in the lower panel. Reproduced from H. Takano, J. R. Kenseth, S.-S. Wong, J. C. O'Brien, M. D. Porter,* Chem. Rev. *99 (1999) 2845.*

Table 2.3 *Scanning probe techniques and the properties they probe.*

Technique	Property probed
Contact mode	
Atomic force microscopy	van der Waals forces, chemical forces, electrostatic interactions, topography
Infrared atomic force microscopy	infrared absorption, thermal expansion
Near-field microwave microscopy	microwave losses
Nano-impedance spectroscopy	interface potential, capacitance, dopant profiling
Piezoforce microscopy	switching dynamics, relaxation time, domain nucleation
Scanning capacitance force microscopy	dopant profile
Scanning capacitance microscopy	capacitance, relative dopant density
Scanning near-field optical microscopy	frequency-dependent dielectric function, surface polaritons, Rayleigh scattering, IR absorption, fluorescence
Scanning non-linear microscopy	dielectric constant
Scanning spreading resistance microscopy	resistivity, relative doping density
Non-contact mode	
Atomic force microscopy	van der Waals forces, chemical forces, electrostatic interactions, topography
Electrostatic force microscopy	electrostatic force
Kelvin force microscopy	potential, work function, adsorbate enthalpy and entropy
Magnetic force microscopy	magnetic force
Microwave-frequency ac STM	polarizability, dopant profile, dielectric response
Photoinduced force microscopy	linear or nonlinear absorption of light, stimulated Raman scattering, optical polarizability, excited state lifetime
Scanning gate microscopy	current flow, local band energy, contact potential variation
Scanning impedance microscopy	interface potential, capacitance, local band energy, current flow
Scanning tunnelling microscopy	topography; local density of states; mapping of gate voltage, bias, and magnetic field; dispersion; phonon and spin excitation; spatial spin contract
Tip-enhanced Raman scattering	Raman scattering

Adapted from Bonnell et al. [24].

Optical and electron microscopy

Optical microscopy

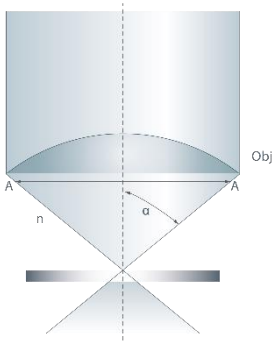

• Limit of resolution(δ): mainly by the wavelength λ of the light

$$\delta = \lambda / 2n \sin \alpha$$

α: the angular aperture (half the angle subtended at the object by the objective lens),
n: the refractive index of the medium between the object and the objective lens,
n sin α: the numerical aperture of the objective lens for a given immersion medium

Numerical aperture: generally less than unity
up to 1.5 with oil-immersion objectives → 600 nm light: 200 nm (0.2 μm) resolution limit

Serious error in particle size less than 2 μm (Table 3.1)

Table 3.1 Determination of the diameters of spherical particles by optical microscopy[29]

True diameter/μm	*Visual estimate/μm*
1.0	1.13
0.5	0.68
≤ 0.2	0.5

• Limitation: resolution power & contrast

Transmission electron microscopy(TEM)

- e-beam: wavelength λ ~ 0.01 nm
- resolution: 0.2 nm
- limitation: high vacuum system

Scanning electron microscopy(SEM)

- resolution: ~ 5 nm

SEM

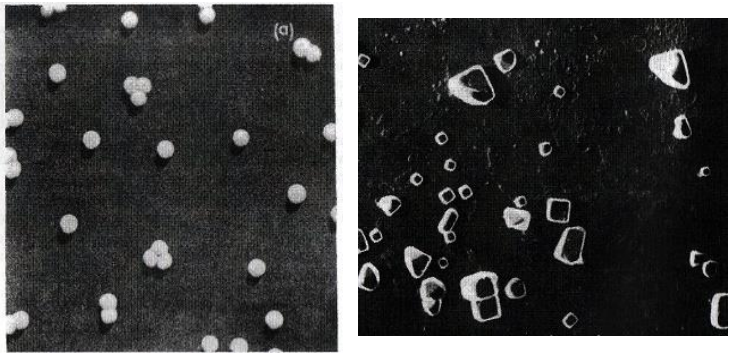

Figure 3.2 Electron micrographs. (a) Shadowed polystyrene latex particles (×50 000). (b) Shadowed silver chloride particles (× 15 000)

Near-field scanning optical microscopy (NSOM or SNOM)

a small-diameter optical fiber close to the surface (diameter/distance < wavelength of the light) → image resolution far below light wavelength (can be exceeded by using near-field technique)

Optical fiber + laser + AFM techniques
Resolution ~ 50 nm, ultimate resolution ~ 12 nm
(By working close enough to the aperture, resolution close to the size of the aperture and far below the wavelength of the light can be obtained)

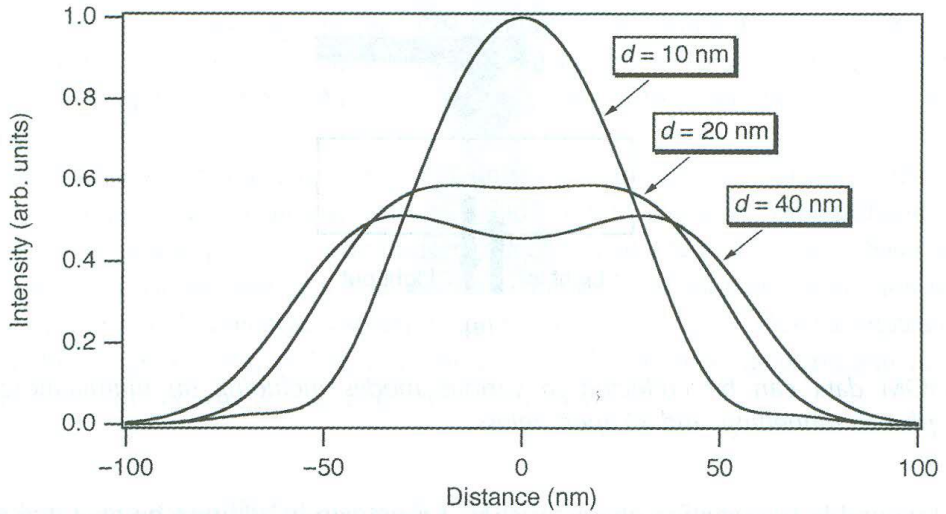

Figure 2.10 *Near-field intensity distributions are shown for 532 nm light that has passed through an aperture with a diameter of 100 nm at distances d from the aperture of 10, 20 and 40 nm. The distributions are normalized such that they all have the same integrated intensity.*

NSOM:
-high brightness of light (laser)
-optical fiber

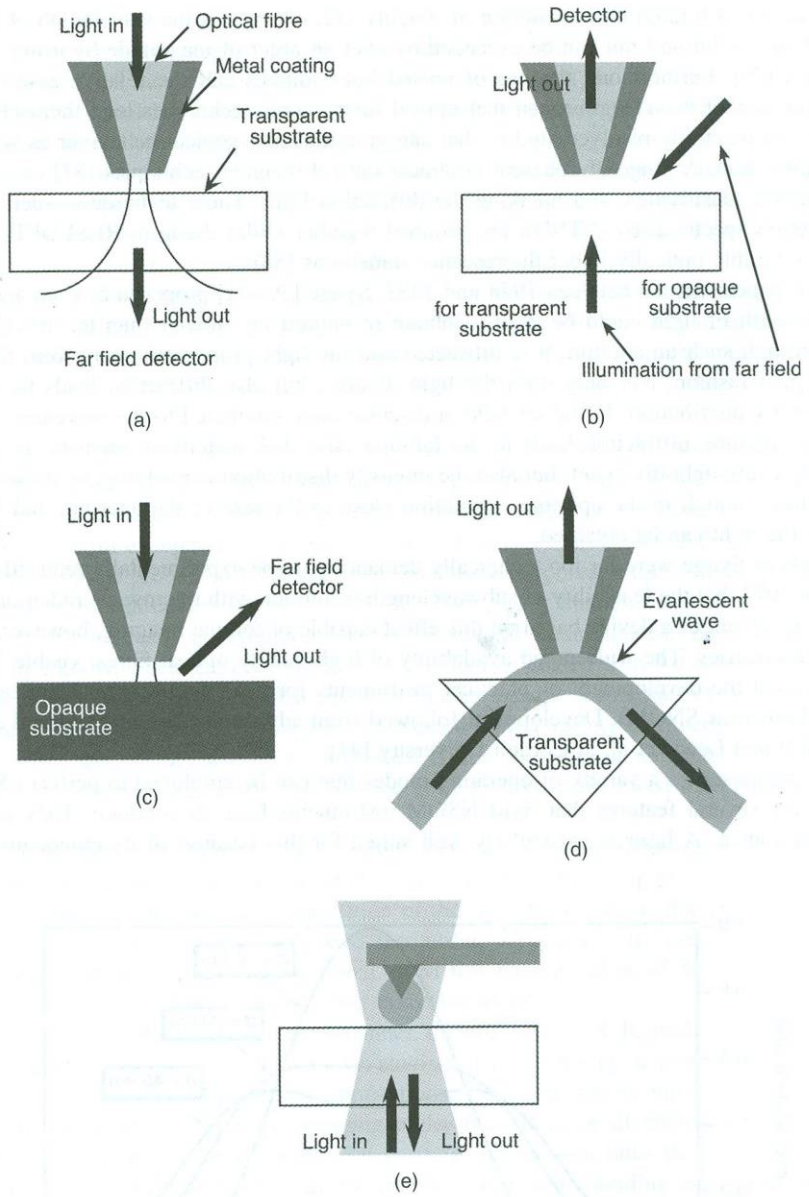

Figure 2.11 NSOM data can be collected in various modes including (a) illumination; (b) collection; (c) reflection; (d) photon tunnelling; and (e) apertureless.

Small aperture diameter (typically 80~100 nm) → few tens of nW light power → ultimate resolution ~12 nm (practically ~50 nm)

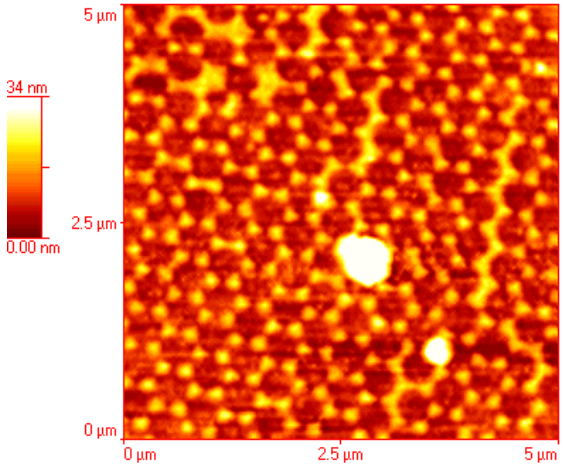

elchem.kaist.ac.kr

Second harmonic and sum frequency generation

SHG & SFG are two closely related techniques → application in surface and interface science → laser light illuminates an interface between two phases A and B → excites a non-linear polarization responses

1) Two photons at same frequency ω, can be mixed together to form a 3rd photon at frequency $\omega = \omega_1 + \omega_2$

→ "second harmonic generation"

2) Two photons with distinct frequencies ω_1 and ω_2 and angle of incidence θ_1 and θ_2 can mix together to form 3rd photon $\omega = \omega_1 + \omega_2$ which depart at θ_3

→ "sum frequency generation"

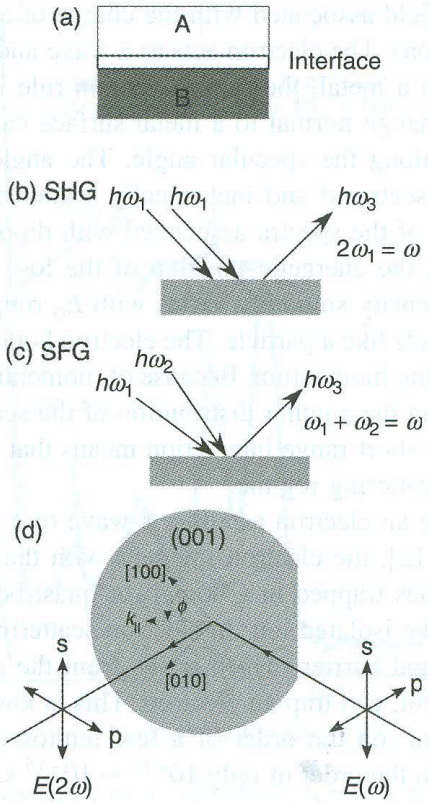

Figure 2.30 *(a) Two bulk materials joined by an interfacial region. (b) Two photons of the same frequency are mixed in second harmonic generation (SHG). (c) Two photons of different frequency are mixed in sum frequency generation (SFG). (d) The polarization components* s *and* p *are shown for a laser incident on a surface.*

Second harmonic spectroscopy

Second harmonic generation (SHG): $\omega \rightarrow 2\omega$
Second harmonic generation (SHG): noncentrosymmetric crystals
If symmetry is broken at the solid/liquid interface → SHG signal

SHG signal is sensitive to species at the interface: used to detect adsorbed species, reaction intermediates etc